2018

Examination Of Callaway-Holland-Based Thermal Conductivity Calculation For Nano-Phononic Crystals

Ruiyuan Ma
University of Pennsylvania, ruiyuanma@gmail.com

Examination Of Callaway-Holland-Based Thermal Conductivity Calculation For Nano-Phononic Crystals

Abstract
Phononic crystals are periodic structured materials whose frequency spectrum is characterized by band gaps, which are regions in frequency space where acoustic or elastic waves cannot propagate. Nano scale phononic crystals have shown promise for reducing thermal conductivity and improving the thermoelectric figure of merit. Correctly calculating the thermal conductivity of nano phononic crystals has become increasingly important due to the growing research interest in the thermal properties of these materials. A widely used expression to calculate thermal conductivity, presented by Klemens and expressed in terms of the relaxation time by Callaway and Holland, originates from the Boltzmann transport equation. In its most general form, this expression involves a direct summation of the heat current contributions from individual phonons of all wavevectors and polarizations in the first Brillouin zone. In common practice, the expression is simplified by three assumptions commonly applied in bulk materials: first, the isotropic assumption that converts the summation over wavevector to an integral over wavevector magnitude; second, the assumption that phonon-phonon scattering rates for nano-phononic crystals can be described by the same empirical expressions commonly used for bulk materials and fitted to experimental data in bulk materials; third, the effective material assumption that the thermal transport can be modeled by treating the nano-phononic crystal as a single bulk effective medium with properties dictated by the nano-phononic crystal dispersion relation. The accuracy of nano-phononic crystal thermal conductivity predictions using these three assumptions need to be validated. In this dissertation, we propose to verify these assumptions one by one.

First, to investigate the isotropic assumption, the thermal conductivities of bulk Si, Si/Ge superlattices, and Si/Ge quantum dot superlattices have been calculated using both the isotropic and direct summation methods, and the results show that the differences between the two methods increase substantially with supercell size. These differences arise because the vibrational modes neglected in the isotropic assumption provide an increasingly important contribution to the thermal conductivity for larger supercells. To avoid the significant errors that can result from the isotropic assumption, direct summation is recommended for thermal conductivity calculations in superstructures. Second, to investigate the assumption of the empirical phonon-phonon scattering rates from bulk material, work to calculate the phonon-phonon scattering rates from the empirical equations has been done and compared against the results from an established normal mode analysis method, which provides more accurate results. The fundamental reasons behind the difference between the empirical method and the NMA method will be discussed. Finally, the effective material assumption will be briefly examined by using Green Kubo Modal Analysis method. Overall, this dissertation will provide direction in the correct thermal conductivity calculation for nano-phononic crystals.

Degree Type
Dissertation

Degree Name
Doctor of Philosophy (PhD)

Graduate Group
Mechanical Engineering & Applied Mechanics

EXAMINATION OF CALLAWAY-HOLLAND-BASED THERMAL CONDUCTIVITY CALCULATION FOR NANO-PHONONIC CRYSTALS

Ruiyuan Ma

A DISSERTATION

in

Mechanical Engineering and Applied Mechanics

Presented to the Faculties of the University of Pennsylvania

in

Partial Fulfillment of the Requirements for the

Degree of Doctor of Philosophy

2018

Supervisor of Dissertation

Jennifer Lukes, Professor
Department of Mechanical Engineering and Applied Mechanics

Graduate Group Chairperson

Kevin Turner, Professor
Department of Mechanical Engineering and Applied Mechanics

Dissertation Committee:
Celia Reina, Assistant Professor
Department of Mechanical Engineering and Applied Mechanics

Portonovo S. Ayyaswamy, Asa Whitney Professor
Department of Mechanical Engineering and Applied Mechanics

EXAMINATION OF
CALLAWAY-HOLLAND-BASED THERMAL
CONDUCTIVITY CALCULATION FOR
NANO-PHONONIC CRYSTALS

To my sister: Ruili Ma

– a great sister, a brilliant lawyer, a brave mother

Gate, Gate, Paragate, Parasamgate, Bodhi Svaha!

Acknowledgments

I would like to thank Professor Jennifer R. Lukes for proposing and guiding this project and giving me the opportunity of studying at Penn. I would also like to thank Professor Portonovo S. Ayyaswamy and Professor Celia Reina for serving on my dissertation committee.

I am very thankful for the support given to me by the current and former members of Professor Lukes research group: Paul Barclay, Joseph Cooke, Masahiro Narasaki, Mehdi Zanjani, and Drew Cheney. I am also thankful to those people I have met at Penn or outside of Penn.

Finally, I would like to thank my family and friends: My parents, Fuyan Ma and Qiulian Zhang; My siblings and their families: Ruili Ma, Ruibing Ma, Zhuoqun Ma, Zhuoran Ma, Zecheng Fan, Zexi Fang; Uncles and Aunts: Fujun Ma, Fuyun Ma; Dr Yiming Cheng.

This work has been funded by the National Science Foundation and the Office of Naval Research.

ABSTRACT

EXAMINATION OF CALLAWAY-HOLLAND-BASED THERMAL CONDUCTIVITY CALCULATION FOR NANO-PHONONIC CRYSTALS

Ruiyuan Ma

Jennifer R. Lukes

Phononic crystals are periodic structured materials whose frequency spectrum is characterized by band gaps, which are regions in frequency space where acoustic or elastic waves cannot propagate. Nano scale phononic crystals have shown promise for reducing thermal conductivity and improving the thermoelectric figure of merit. Correctly calculating the thermal conductivity of nano phononic crystals has become increasingly important due to the growing research interest in the thermal properties of these materials. A widely used expression to calculate thermal conductivity, presented by Klemens and expressed in terms of the relaxation time by Callaway and Holland, originates from the Boltzmann transport equation. In its most general form, this expression involves a direct summation of the heat current contributions from individual phonons of all wavevectors and polarizations in the first Brillouin zone. In common practice, the expression is simplified by three assumptions commonly applied in bulk materials: first, the isotropic assumption that converts the summation over wavevector to an integral over wavevector magnitude; second, the assumption that phonon-phonon scattering rates for nano-phononic crystals can be described by the same empirical expressions commonly used for bulk materials and fitted to experimental data in bulk materials; third, the effective material assumption that the thermal transport can be modeled by treating the nano-phononic crystal as a single bulk effective medium with properties dictated by the nano-phononic crystal dispersion relation. The accuracy of nano-phononic crystal thermal conductivity predictions using these three assumptions need to be validated. In this dissertation, we propose to verify these assumptions one by one.

First, to investigate the isotropic assumption, the thermal conductivities of bulk Si, Si/Ge superlattices, and Si/Ge quantum dot superlattices have been calculated using both the isotropic and direct summation methods, and the results show that the differences between the two methods increase substantially with supercell size. These differences arise because the vibrational modes neglected in the isotropic assumption provide an increasingly important contribution to the thermal conductivity for larger supercells. To avoid the significant errors that can result from the isotropic assumption, direct summation is recommended for thermal conductivity calculations in superstructures. Second, to investigate the assumption of the empirical phonon-phonon scattering rates from bulk material, work to calculate the phonon-phonon

scattering rates from the empirical equations has been done and compared against the results from an established normal mode analysis method, which provides more accurate results. The fundamental reasons behind the difference between the empirical method and the NMA method will be discussed. Finally, the effective material assumption will be briefly examined by using Green Kubo Modal Analysis method. Overall, this dissertation will provide direction in the correct thermal conductivity calculation for nano-phononic crystals.

Contents

Contents vii

List of Tables ix

List of Figures x

1 Introduction 1
- 1.1 Nano-Phononic Crystals . . . 1
- 1.2 Applications in Tailoring Thermal Conductivity . . . 2
- 1.3 Thermal Conductivity Calculation Methods . . . 2
  - 1.3.1 Molecular Dynamics . . . 3
  - 1.3.2 The Phonon BTE Equation . . . 4
- 1.4 Group Velocity and Relaxation Times . . . 10
  - 1.4.1 Harmonic Lattice Dynamics . . . 10
  - 1.4.2 Anharmonic Lattice Dynamics . . . 11
  - 1.4.3 Normal Mode Analysis . . . 11
- 1.5 Thermal Conductivity Calculation of Periodic Materials . . . 14
  - 1.5.1 Superlattices . . . 14
  - 1.5.2 Phononic Crystals . . . 15
- 1.6 Thermal Conductivity Calculation in Nano-Phononic Crystals: Problems and Assumptions . . . 15
- 1.7 Goals . . . 17

2 Examination of the Isotropic Thermal Conductivity Assumption for Nano-Phononic Crystals 18
- 2.1 Literature Reviews on Isotropic Assumption . . . 18
- 2.2 Methods to Validate the Assumption . . . 20
  - 2.2.1 Theory and Methods . . . 20
- 2.3 Results . . . 23
  - 2.3.1 Verification of Modeling Methods . . . 24
  - 2.3.2 Bulk Silicon . . . 24
  - 2.3.3 Silicon/Germanium Quantum Dot Superlattices . . . 26
- 2.4 Discussion . . . 27
- 2.5 Conclusions . . . 33

3 Examination of the Empirical Relaxation Time Assumption for Nano-Phononic Crystals **35**
3.1 Literature Reviews . . . 36
3.1.1 Empirical Relaxation Time Equations . . . 36
3.1.2 Non-Empirical Relaxation Times . . . 36
3.2 Methods to Validate the Assumption . . . 38
3.3 Results . . . 39
3.3.1 Verification of Modeling Methods . . . 39
3.3.2 Bulk Materials . . . 40
3.3.3 Nano-Phononic Crystals . . . 43
3.4 Discussion . . . 46
3.5 Conclusions . . . 52

4 Examination of the Effective Material Assumption for Nano-Phononic Crystals **54**
4.1 Literature Reviews on Previous Work . . . 55
4.1.1 Optical Meta-Material Versus Photonic Crystals . . . 55
4.1.2 Virtual Crystal Assumption . . . 55
4.1.3 Introduction of GKMA Method . . . 56
4.2 Method to Validate the Assumption . . . 57
4.3 Results . . . 57
4.3.1 Verification of GKMA method . . . 57
4.3.2 Nano-Phononic Crystals . . . 58
4.4 Conclusion . . . 61

5 Conclusions **62**
5.1 Summary and Contributions . . . 62
5.2 Challenges . . . 63
5.3 Future Directions . . . 64

Appendix **64**

A Group Velocity **65**

Bibliography **65**

List of Tables

1.1 Thermal Conductivity Methods Used in the Present Work 13

2.1 Simulation parameters 23

3.1 Empirical equations of inverse relaxation time for different scattering processes (adapted from Feng & Ruan (2014)) 37
3.2 Simulation parameters for Ar/Heavy Ar QDSLs with mass ratio of 3 . 40

4.1 Thermal conductivity from GKMA and NMA methods $[W/mK]$ . . . 61

List of Figures

2.1 Schematic of Si3Ge1 quantum dot superlattice. The silicon supercell is the central cube with black boundaries. It has a side length of 3 CCs and is embedded with a blue germanium quantum dot with side length 1 CC. The supercell is repeated infinitely in all directions, as indicated by the neighboring "image" supercells with faint gray quantum dots. 21
2.2 (a) Spherical Brillouin zone and (b) Neglected phonons. 23
2.3 (a) Reduced thermal conductivity for Si, Ge and Si/Ge superlattices with different periodicity; (b) Thermal conductivity for bulk Si. Lines are results from this work, markers in (a) are results from Ref. (Tamura et al. 1999), and markers in (b) are results from Ref. (Hopkins et al. 2009). 24
2.4 Thermal conductivity of bulk Si with different supercell sizes using the direct summation and isotropic methods. 25
2.5 Thermal conductivity of (a) Si/Ge QDSLs in [100] direction, (b) Ge/Si QDSLs in [100] direction and (c) Si/Ge QDSLs in [110] direction. . . . 27
2.6 Ratio of the isotropic and direct summation results in bulk Si, Si/Ge QDSLs, and Ge/Si QDSLs along the [100] direction. 28
2.7 Ratios of the Brillouin shape effect ($k_{FBZ} - k_{SBZ}$) and the anisotropic effect ($k_{SBZ} - k_{ISO}$) to the direct summation result (k_{FBZ}) in Si/Ge and Ge/Si QDSLs along the [100] direction. 30
2.8 Real space representations and Brillouin zones for supercell with (a) $2 \times 2 \times 2$ CCs and (b) $4 \times 4 \times 4$ CCs. 31
2.9 (a) Ratio of average value from neglected and all phonons in [110] direction in bulk Si, and (b) ratio of isotropic assumption result to full Brillouin zone result in bulk Si using three different τ expressions. . . 32
2.10 Normalized branch averaged $\langle \tau(q) \rangle$ in [110] direction for different bulk silicon supercell sizes. 32
2.11 Percentage contribution of neglected phonons to thermal conductivity in Si/Ge and Ge/Si QDSLs along the [100] direction. 33

3.1 Verification of the normal mode analysis method to literature results: Blue stars are result from current work, red circles is result from the reference paper (Huberman 2013). The geometry is Ar heavy Ar superlattices with thickness of 4CCs and length 8x6x6 at T=20K. . . . 39

3.2 Convergence test of bulk Ar for different sizes: (a) bulk Ar 40x10x10 CCs and (b) bulk Ar 60x10x10 CCs. 41
3.3 Convergence test of bulk Ar for different time intervals in MD: (a) time interval = 32 time steps and (b) time interval = 16 time steps using bulk Ar 40x10x10 CCs. 42
3.4 Convergence test of velocity in bulk Ar for different q-space resolutions with dq = 10^{-5}, $5x10^{-5}$, and $10x10^{-5}$. 42
3.5 Lifetime of bulk Ar using the normal mode analysis method. 43
3.6 Thermal conductivity of bulk Ar with different supercell sizes using the empirical equation and normal mode analysis methods. 44
3.7 Thermal conductivity of Ar/Heavy-Ar QDSL with (different) dot masses using the empirical equation and normal mode analysis methods. . . 45
3.8 The ratio of thermal conductivity results from the empirical equation method and the normal mode analysis method for Ar/H-Ar QDSL with different dot masses. 45
3.9 Lifetime of Ar/Heavy-Ar QDSL using the empirical equation method (green circles) and normal mode analysis method (blue circles) with different mass ratio: (a) mass ratio = 2, (b) mass ratio = 3, (c) mass ratio = 4, and (d) mass ratio = 5. 46
3.10 The difference of cumulative mode thermal conductivity between two methods, χ, as function of frequency for different mass ratios. 48
3.11 The difference of cumulative mode lifetime between two methods, χ_τ as a function of frequency for different mass ratios. 48
3.12 The normalized cumulative values of mode Cp, Φ_{C_p}, as a function of frequency for different mass ratios. 49
3.13 The normalized cumulative values of mode v_x^2, $\Phi_{v_x^2}$, as a function of frequency for different mass ratios. 50
3.14 The summation of Cp for different mass ratio. 50
3.15 The summation of v^2 for different mass ratio. 51
3.16 The summation of τ from empirical equation and NMA methods for different mass ratio. 51
3.17 The dispersion curve of Ar/Heavy Ar QD (2x2x2 CCs and mass ratio = 5) with a mini-bandgap at [7.1 - 8.1] frequency range. 52

4.1 Heat current autocorrelation function (top) and thermal conductivity (bottom) of GKMA method for bulk Ar with 6x6x6 CCs at T = 20 K. 58
4.2 Thermal conductivity of GKMA method for bulk Ar at T=50K using a 4x4x4 conventional cell. Bold magenta line is the average thermal conductivity of five initializations. 59
4.3 Thermal conductivity of GKMA method for Ar/heavy Ar with 3x3x3-2x2x2 CCs at T = (a) 20 K, (b) 30 K, (c) 40 K, and (d) 50 K. 60

A.1 Phonon group velocities from different branches along the [100] direction in (a) bulk Si with 1x1x1 CCs and (b) Si3Ge1 QDSL. 65

Chapter 1

Introduction

1.1 Nano-Phononic Crystals

Nano-phononic crystals, which are composite materials with nanoscale structural periodicity, have attracted considerable attention in recent years due to their unusual physical properties (Cargnello et al. 2015, Knight 2003, Wang et al. 2016, Nikitov et al. 2001, Soukoulis & Wegener 2011). Phononic crystals are periodic structured materials whose frequency spectrum is characterized by band gaps, which are regions in frequency space where acoustic or elastic waves cannot propagate. Therefore, phononic crystals have been widely applied to control the propagation of sound and elastic waves (Wang et al. 2014, Graczykowski et al. 2015, Maldovan 2013*b*). In applications ranging from thermoelectric energy harvesting (Martín-González et al. 2013) to advanced thermal insulations (Maldovan 2015), identifying new materials with very low thermal conductivities is essential to advance the state of the art technology. Nano-phononic crystals have shown promising applications in reducing thermal conductivity and improving the thermoelectric figure of merit. In particular, it has been proposed that the nano-phononic crystals with different air holes or pillars can be used to control and suppress the propagation of heat (Tang et al. 2010, Hopkins et al. 2010, Maldovan 2013*a*, Zen et al. 2014, Maldovan 2015, Anufriev & Nomura 2017). It is also well established that superlattices, or planar composites with 1D nanoscale periodicity (1D nano-phononic crystals), can be tailored to achieve low

thermal conductivities (Lee et al. 1997, Koh et al. 2009). The thermal conductivities of such materials can be tuned by varying the periodicities and characteristic sizes of the constituent materials (Tang et al. 2010, Hopkins et al. 2010, Zen et al. 2014, Ravichandran et al. 2014, Yu et al. 2010). This tunability arises from the geometry dependence of the phonon dispersion relation (Yu et al. 2010, Davis & Hussein 2014, Zen et al. 2014) and the interfacial phonon relaxation time (Qiu et al. 2015, Koh et al. 2009). Designing nano-phononic crystals with lower thermal conductivity has been a popular research topic.

1.2 Applications in Tailoring Thermal Conductivity

Nano-phononic crystals have been proposed to be able to tailor thermal conductivity, which attracts a lot of interest. The notable concept in the literature is thermocrystals proposed in 2013 (Maldovan 2013*a*), which could potentially reduce thermal conductivity by 23%. The thermocrystal structure is a combination of nano-phononic crystal and alloy. The silicon thin film was embedded with different air cylinder structures while the substrate was mixed with nano-particles. This hybrid structure was designed to eliminate the transport of phonons in certain frequency ranges. Another pioneering work in tailoring thermal conductivity with nano-phononic crystals (Davis & Hussein 2014) utilized local resonances of nano pillars in the silicon pillar-on-plate nano-phononic crystals to reduce group velocity and thus thermal conductivity in this system.

Since then, tens of papers have been published to tailor thermal conductivity using nano-phononic crystals.

1.3 Thermal Conductivity Calculation Methods

Multiple methods to calculate thermal conductivity have been developed. This section will briefly introduce the most relevant methods.

1.3.1 Molecular Dynamics

The basic idea of molecular dynamics (MD) is to apply Newton's laws of motion on an ensemble of atoms interacting with each other through an interatomic potential. One technique in Molecular Dynamics to study thermal properties is non-equilibrium molecular dynamics (NEMD) or direct method, using a heat source and sink. The other technique is equilibrium molecular dynamics (EMD) which usually uses the formula developed by Green and Kubo (GKMD).

The limitation of molecular dynamics is that it neither considers the quantum effect of a nanoscale system nor simulates the systems behavior under Debye temperature. In addition, this method cannot describe electron-phonon interaction in many semiconductor systems because it is an entirely classical approach, and electrons are not considered.

Equilibrium Molecular Dynamics - Green-Kubo

The GKMD uses fluctuations in the heat current to compute the thermal conductivity in the α direction, as shown in the following equations (Schelling et al. 2002):

$$k_\alpha = \frac{1}{k_B V T^2} \int_0^\infty < S_\alpha(t) \otimes S_\alpha(0) > dt, \tag{1.1}$$

where $S_\alpha(t)$ and $< S_\alpha(t) \otimes S_\alpha(0) >$ are the α component of the heat current vector and the heat current autocorrelation function.

The extensions of Green-Kubo molecular dynamics which used in this dissertation, including normal mode analysis and Green Kubo modal analysis, which will be explained in Chapters 3 and 4.

Non-Equilibrium Molecular Dynamics

Non-Equilibrium Molecular Dynamics (NEMD), which is also called the "direct method", requires a temperature gradient across the simulation cell, while the Green-Kubo approach uses current fluctuations to compute the thermal conductivity via the fluctuation-dissipation theorem. The temperature gradient is created in the simu-

lation system by adding or removing heat from two thin slabs of the same thickness. Even though only kinetic energy is added to the system, equilibration between kinetic and potential energy is expected to be achieved in a typical vibration period. The heat current and the resulting temperature gradient is then calculated when the system reaches steady state, and Fourier's law is used to obtain thermal conductivity.

There are some challenges associated with NEMD. One is the tendency of the center of mass of the entire system to drift. The other one is the size effect from the limited simulation cell size used in this method. Both challenges can be alleviated by carefully design the simulations including using the velocity-rescaling algorithm and extrapolating the behavior of infinite system by performing several simulations with different sizes for the same system.

Homogeneous NEMD

Homogeneous NEMD (Evans 1982) was developed based on an extension of linear response theory for non-canonical, classical systems. This theory allows calculating the thermal conductivity based on a translationally invariant non-equilibrium simulation algorithm for dense fluids. Excellent agreement with experiment is obtained when applied to Lennard-Jones Ar material.

1.3.2 The Phonon BTE Equation

BTE Equation

The BTE equation is based on a different theory from molecular dynamics. The fundamental equation to study the thermal conductivity is the steady state phonon Boltzmann Transport Equation (BTE) (Klemens 1958, Ziman 1960, Kaviany 2014) in the perturbation theory, which describes the balance of phonon population between diffusive drift and scattering as

$$\vec{v}_\lambda \cdot \nabla(n_\lambda) = \frac{\partial n_\lambda}{\partial t}|_s, \tag{1.2}$$

in which $\vec{v}_\lambda$ is the group velocity, λ specifies the phonon mode, $n_\lambda = n^0_\lambda + n'_\lambda$ is the total phonon occupation number with n'_λ representing the deviation from the equilibrium phonon distribution n^0_λ. The big challenge is how to solve for the right hand side scattering term in the Eq. 1.2. With the assumption that n'_λ is independent of temperature, we can get $\nabla(n_\lambda) = (\frac{\partial n_\lambda}{\partial T})\nabla T \simeq (\frac{\partial n^0_\lambda}{\partial T})\nabla T$. The equation 1.2 can be converted to

$$\vec{v}_\lambda \nabla T(\frac{\partial n^0_\lambda}{\partial T}) = \frac{\partial n'_\lambda}{\partial t}|_s. \tag{1.3}$$

In the case of a small thermal gradient, the equation is solved linearly, by considering just small deviation from equilibrium. Let's define Φ_λ as $n_\lambda = n^0_\lambda - \Phi_\lambda \frac{\partial n^0_\lambda}{\partial(\hbar\omega_\lambda)}$ where $\hbar\omega_\lambda$ is the energy of a phonon. The density of the thermal current U can be defined as (Sparavigna 2016)

$$U = \frac{1}{\Omega}\sum_\lambda \hbar\omega_\lambda v_\lambda n_\lambda = -\frac{1}{\Omega}\sum_\lambda \hbar\omega_\lambda v_\lambda \frac{\partial n^0_\lambda}{\partial(\hbar\omega_\lambda)}\Phi_\lambda \tag{1.4}$$

where $\Omega = NV$ is the volume of the crystal, N is the number of primitive cells. The density current U can also be expressed in a Cartesian frame with unit vectors u_i as $U_j = -\sum_i k_{ji}\frac{\partial T}{\partial x_i}$. Tensor k_{ij} is the thermal conductivity tensor.

Iterative Methods

The iterative method is based on an iterative solution to the linearized BTE, was first proposed by Omini and Sparavigna (Omini & Sparavigna 1995, 1996). Instead of calculating the anharmonic corrections to quasi-harmonic frequencies and linewidth, the iterative method uses the phonon scattering probability which are typically computed with Fermi's golden rule (Ziman 1960, Srivastava 1990, Broido et al. 2005). Omini and Sparavinga has computed the thermal conductivity of argon and krypton (Omini & Sparavigna 1996) and silicon and germanium (Omini & Sparavigna 1997). Broido extended this method to calculate the thermal conductivity of bulk silicon and germanium with second- and third-order force constants completely from density functional perturbation theory (DFPT) calculations (Broido et al. 2007). The

iterative method solves the linearized BTE to compute the thermal properties for semiconductor materials, which has been proved as an accurate method (Debernardi et al. 1995, Deinzer et al. 2003, Omini & Sparavigna 1995, 1996, Broido et al. 2005). This computational framework can provide accurate thermal property calculations without adjustable parameters. The iterative method and Fermi's golden rule have then been extensively used in the last decade and have produced thermal properties of polar and non-polar semiconductors with good agreement with experimental measurements, including bulk Si (Broido et al. 2005, Ward & Broido 2010, Esfarjani et al. 2011), Si/Ge superlattice (Garg et al. 2011, Garg & Chen 2013), Mg_2X (Chernatynskiy & Phillpot 2015*a*), graphene and other materials. The main drawback of this method is that it requires a huge computational effort both from the electron energy structure calculation and iterative solution calculations (Omini & Sparavigna 1996).

Here is the brief summary for the iterative method, and details can be found in the reference (Broido et al. 2005). The start point of the iterative method is the energy and quasi-momentum conservation

$$\omega_j(q) \pm \omega_{j'}(q') = \omega_{j''}(q''), q \pm q' = q'' + K, \tag{1.5}$$

where j is the phonon branch index, and K is a reciprocal lattice vector that is zero for normal processes and nonzero for umklapp processes. The branch index (j, q) is same as λ.

The equation $n'_\lambda = -\frac{\partial n^0_\lambda}{\partial \omega_\lambda}\Psi_\lambda$ is used to perturb the phonon distribution function n_λ, where Ψ_λ represents the deviation from the equilibrium distribution function. Using the $\delta(\omega_\lambda \pm \omega_{\lambda'} - \omega_{\lambda''})$ function to maintain the conservation of energy and momentum, the three-phonon scattering rates can be written as

$$W^{\pm}_{\lambda\lambda'\lambda''} = \frac{\pi}{4N}\frac{n^0_\lambda(n^0_{\lambda'} + 1/2 \pm 1/2)(n^0_{\lambda''} + 1)}{\omega_\lambda\omega_{\lambda'}\omega_{\lambda''}}|\Phi_\pm(\lambda, \lambda', \lambda'')|^2 \times \delta(\omega_\lambda \pm \omega_{\lambda'} - \omega_{\lambda''}), \tag{1.6}$$

where N is the number of unit cells. To measures the strength of scattering events, the three-phonon scattering matrix elements, $\Phi_\pm(\lambda, \lambda', \lambda'') = \Phi(j, -q; j', \mp q'; j'', q'')$, is

described by

$$\Phi(j,-q;j',\mp q';j'',q'') = \sum_{m}\sum_{l'm'}\sum_{l''m''}\sum_{\alpha\beta\gamma}\Phi_{\alpha\beta\gamma}(0m,l'm',l''m'') \times e^{\iota q'\cdot R_{l'}}e^{\iota q''\cdot R_{l''}}\frac{\vec{e}^{\,j}_{\alpha m}(q)\vec{e}^{\,j'}_{\beta m'}(q')\vec{e}^{\,j''}_{\gamma m''}(q'')}{\sqrt{M_m M_{m'} M_{m''}}}, \tag{1.7}$$

where $0, l', l''$ are the unit cells of the three atoms, m, m', m'' specify the atoms in the corresponding unit cells whose mass are $M_m, M_{m'}, M_{m''}$, and α, β, γ are Cartesian components. $\Phi_{\alpha\beta\gamma}(0m, l'm', l''m'')$ is the third-order force constant, and the $\vec{e}$ represent phonon eigenvectors. The scattering rate from isotropic impurities ($W^{imp}_{\lambda\lambda'}$) and boundary ($W^{bs}$) can also be found in the reference paper (Broido et al. 2005). The linearized phonon Boltzmann equation can be converted into

$$\begin{aligned} k_B T\cdot\vec{v}_\lambda\nabla T\left(\frac{\partial n^0_\lambda}{\partial T}\right) &= \sum_{\lambda'\lambda''}\left[W^{+}_{\lambda\lambda'\lambda''}\left(\Psi_{\lambda''}-\Psi_{\lambda'}-\Psi_\lambda\right)+\right. \\ &\left.\frac{1}{2}W^{-}_{\lambda\lambda'\lambda''}\left(\Psi_{\lambda''}+\Psi_{\lambda'}-\Psi_\lambda\right)\right] \\ &+\sum_{\lambda'}W^{imp}_{\lambda\lambda'}\left(\Psi_{\lambda'}-\Psi_\lambda\right)-n^0_\lambda\left(n^0_\lambda+1\right)\Psi_\lambda\frac{1}{\tau^{bs}}. \end{aligned} \tag{1.8}$$

In order to solve Eq. (1.8) using the iterative method, it's necessary to define $\Psi_\lambda = \sum_\lambda F_{\lambda\alpha}(\partial T/\partial x_\alpha)$ and substitute it into Eq. (1.8), three new equations will be obtained and the iterative procedure can be initiated by following the details in the reference paper (Broido et al. 2005).

The RTA Assumption

The relaxation time assumption is commonly used to solve equation 1.3, which assumes that deviation of single phonon mode population has an exponential decay curve with time:

$$n'_\lambda \propto \exp\left(-\frac{t}{\tau_\lambda}\right), \tag{1.9}$$

where τ_λ represents the relaxation time. The right hand side (the collision term) in BTE (1.3) becomes

$$\frac{\partial n'_\lambda}{\partial t}|_s \simeq -\frac{n'_\lambda}{\tau_\lambda}. \tag{1.10}$$

Therefore, the steady state BTE (1.2) under the RTA assumption can be expressed as

$$\vec{v}_\lambda \nabla T \left(\frac{\partial n^0_\lambda}{\partial T}\right) = -\frac{n'_\lambda}{\tau_\lambda}. \tag{1.11}$$

The relaxation time, $\tau_\lambda = 1/\Gamma_\lambda$ where Γ_λ is the scattering rate, is interpreted as the average time between collisions of the phonon mode λ with other modes. Incorporating the Bose-Einstein distribution in Eq. (1.11), we can get a simple model to calculate phonon thermal conductivity (Klemens 1958), which is also called the direct summation method in this work,

$$k_{FBZ} = \sum_\lambda C_{ph}(\vec{q},\lambda) v^2(\vec{q},\lambda) \tau(\vec{q},\lambda) \tag{1.12}$$

where $\vec{q}$ is wavevector. The summation is taken over all phonons in the full Brillouin zone, as noted by the subscript FBZ. All the parameters, $C_{ph}, k_B, \hbar, T, \omega$, has been defined in section **??**.

Analytical Models (the Callaway-Holland Model)

Multiple analytical models have been developed based on the phonon BTE equations, in which the Callaway-Holland model (Callaway 1959, Holland 1963) is the most commonly used. The Callaway-Holland model is based on the RTA assumption (Eq. (1.11)), however, it segmented scattering processes into two categories: the processes which conserve the total crystal momentum (the normal processes), and the processes which do not conserve the crystal momentum including umklapp processes, impurity scattering, and boundary scattering (Callaway 1959). In the original derivation process (Callaway 1959), Callaway only considered the momentum conserving

(N) and non-conserving processes (U), and the Eq. (1.10) can be re-written as:

$$\frac{\partial n'_\lambda}{\partial t}|_s = \frac{n'_\lambda}{\tau_N} + \frac{n'_\lambda}{\tau_U}. \tag{1.13}$$

When τ_N is large enough, the thermal conductivity is determined principally by τ_U and relaxation times from other scattering processes (Callaway 1959). To take other scattering processes (boundary (B) scattering and impurity (I) scattering) into account, the Callaway-Holland model (Callaway 1959) uses the Matthiessen's rule to calculate the total scattering rate τ

$$1/\tau = 1/\tau_U + 1/\tau_B + 1/\tau_I. \tag{1.14}$$

Therefore, the Normal processes relaxation time will not be included in the thermal conductivity calculation in this work.

In order to calculate the thermal conductivity, phonon properties including phonon frequency w, group velocity v, and relaxation time τ need to be input into Eq. (1.12) or Eq. (1.15). The typical Callaway-Holland method used empirical scattering rates, which will be examined in section 3. The most common method to calculate w, v is the lattice dynamics method (LD).

Isotropic Assumption

To make the Callaway-Holland model even simpler, people often use the isotropic thermal conductivity assumption in bulk materials. This assumption assumes that the dispersion curves in all directions are same as the selected directions, such as [100] direction. The general form under RTA assumption, Eq. 1.12 can be written as:

$$k_{ISO} = \frac{1}{6\pi^2} \int_{q=0}^{q_{max}} C_{ph}(q,\lambda) v^2(q,\lambda) \tau(q,\lambda) q^2 dq \tag{1.15}$$

where C_{ph}, q, v, and τ are specific heat, wavevector magnitude in a chosen direction, component of phonon group velocity in the direction of interest, and the phonon relaxation time. λ specifies the phonon branch index. The integration assumes the dis-

persion curves in all directions are same as that in the direction of interest (usually the [100] direction), contrasting to the full dispersion curve which will be introduced in Eq. (1.12) section 1.3. The specific heat is given as $C_{ph}(q,\lambda) = k_B x^2 \exp(x)/(\exp(x)-1)^2$, where $x = \hbar\omega(q,\lambda)/k_B T$ and k_B, $\hbar$, T, and ω are Boltzmann's constant, reduced Planck's constant, temperature, and angular frequency.

Compared to Eq. 1.12, the equation under isotropic assumption uses volume integration instead of direct summation of all phonon modes in the Brillouin zone.

1.4 Group Velocity and Relaxation Times

The group velocity of phonon modes can be represented by the following equation (Landry 2009):

$$v_g(q,\lambda) = \frac{\partial\omega(q,\lambda)}{\partial q} \tag{1.16}$$

The basic method to get the group velocity is to calculate the slopes of the phonon dispersion curve. As for group velocity in x direction, one can make a little change of wavenumber in x direction and keep the same k_y, k_z value and get the derivation of frequency with respect to wavenumber.

It becomes very critical to calculate τ_λ. There are multiple ways for the relaxation times calculation, including empirical equations in harmonic lattice dynamics, anharmonic lattice dynamics, and normal mode analysis. Those methods will be explained in this section.

1.4.1 Harmonic Lattice Dynamics

The lattice dynamics techniques (LD), which is formally derived in the reference book (Dove 1993), gives an approximate analytical solution of the dynamics of the atoms in a crystal. LD techniques can be used differently under two different assumptions, one is harmonic LD and the other is anharmonic LD. The harmonic LD is the most commonly used method to compute the vibrational frequencies and modes available in a crystal lattice. The phonon dispersion curves and density of states (DOS) can

be directly calculated using this method. The main drawback of the harmonic LD is that the atoms in a crystal are assumed to sit at their zero temperature equilibrium positions, which is only valid if the atomic motion is small compared to the spacing between neighboring atoms (Turney 2009). Due to thermal expansion, the spacing between the neighboring atoms can change with temperature, which is one issue related to the harmonic approximation.

1.4.2 Anharmonic Lattice Dynamics

Compared to the analytical models, other accurate calculation methods have been developed in the last decade, such as the Anharmonic Lattice Dynamics (ALD) and the iterative method to solve linearized BTE.

Anharmonic Lattice Dynamics is the natural extension of quasi-harmonic lattice dynamics. Higher (third- and fourth-) order derivatives are included as a perturbation to the quasi-harmonic frequencies in anharmonic LD, which has been fully developed by Turney and *et al.* (Turney 2009). The most important parameters in Anharmonic LD are the frequency shift, Δ , and the linewidth, $\Gamma = 1/\tau_\lambda$, for each phonon mode due to anharmonic interaction with other phonons. The Anharmonic LD addressed the thermal expansion problem in the harmonic LD method by including higher (usually third- and fourth-) order derivatives of the energy as a perturbation to the quasi-harmonic frequencies (Turney 2009). The drawbacks of the anharmonic LD method is that the computation is very complicated and expensive and there are only a few papers published using this method.

1.4.3 Normal Mode Analysis

The normal mode analysis (NMA) method is developed by McGaughey and Kaviany (McGaughey & Kaviany 2005), Turney et al. (Turney 2009), and Larkin et al. (Larkin & McGaughey 2013), based on the data from GKMD. Although it uses the empirical potentials in the classical MD calculation, it provides advantages over other methods such as DFPT and ALD because the molecular dynamics includes the complete

anharmonicity. We briefly review this method in this section and the detailed steps can be found in the reference paper (Huberman 2013). The thermal conductivity calculation equation is similar to the previous k_{FBZ} equation in section 1.12. The main difference is that the phonon life time in the NMA method is extracted from the autocorrelation of total energy of normal modes, which can be defined in the following equation:

$$\tau(\vec{q},\lambda) = \int_0^\infty \frac{< E(\vec{q},\lambda;t)E(\vec{q},\lambda;0) >}{< E(\vec{q},\lambda;t)E(\vec{0},\lambda;0) >}, \tag{1.17}$$

in which the total energy of normal mode can be defined by

$$E(\vec{q},\lambda;t) = \frac{1}{2}\omega(\vec{q},\lambda)Q^*(\vec{q},\lambda;t)Q(\vec{q},\lambda;t) + \frac{1}{2}\dot{Q}^*(\vec{q},\lambda;t)\dot{Q}(\vec{q},\lambda;t), \tag{1.18}$$

where $Q(\vec{q},\lambda;t)$ is the normal mode coordinate (McGaughey & Larkin 2014, Larkin 2013), t is time in MD simulation, and $\vec{q}$ and λ are phonon wave-vector and branch index.

The $\dot{Q}(\lambda,t)$ is the time derivative of the harmonic coordinate, $Q(\lambda,t)$, which are described in the following equations:

$$Q(\lambda,t) = \frac{1}{\sqrt{N}}\sum_{b,l}^{max}\sqrt{m_b}exp[-\iota\vec{q}\cdot\vec{r}(b,l)]\vec{e}^*(\lambda,b)\cdot\vec{u}(b,l,t), \tag{1.19}$$

and

$$\dot{Q}(\lambda,t) = \frac{1}{\sqrt{N}}\sum_{b,l}^{max}\sqrt{m_b}exp[-\iota\vec{q}\cdot\vec{r}(b,l)]\vec{e}^*(\lambda,b)\cdot\dot{\vec{u}}(b,l,t), \tag{1.20}$$

where $\vec{e}(\lambda,b)$ is the eigenvector determined from the harmonic lattice dynamics calculation, and $\vec{u}(b,l,t)$ is the displacement from equilibrium of the atom b in the unit cell l at time t.

The NMA method could also be applied in the frequency domain, which utilizes the relationship between lifetime and the linewidth, $\tau_\lambda = 1/\Gamma_\lambda$, where Γ_λ (same as $\Gamma_{q,v}$). The following equations (Huberman et al. 2013) based on the Lorentzian fitting centered at $\omega_A(\lambda)$:

$$C(\lambda,\omega) = \frac{C_0(\lambda)}{2}\frac{\Gamma(\lambda)/\pi}{(\omega_A(\lambda)-\omega)^2+\Gamma^2(\lambda)}, \tag{1.21}$$

in which $C(\lambda,\omega)$ is the autocorrelation of the normal modes based on the spectral energy density method (SED).

This dissertation used the normal mode analysis in the time domain. The normal mode analysis method can be summarized into six steps: first, create the appropriate atomic structure based on the unit cell needed; second, select the necessary wave-vectors for the super cell; third, calculate the frequencies and mode eigenvectors of the normal phonon modes using harmonic lattice dynamics softwares (GULP); fourth, extract the positions and velocities for all atoms from the Green Kubo molecular dynamics simulation using LAMMPS; fifth, obtain all phonon normal mode coordinates using harmonic lattice dynamics and molecular dynamics; sixth, compute the phonon properties using the autocorrelation of the total normal mode energies for time domain analysis.

Before we move to the next session, let's summarize the thermal simulation method used in this dissertation, as shown in Table 1.1.

Table 1.1: Thermal Conductivity Methods Used in the Present Work

	Callaway-Holland	NMA	GKMA
Relaxation times	Fit from experimental data	Mode autocorrelation functions	N/A
Inputs	ω, τ, group velocity	Forces, eigenvectors and atom velocities from MD	Phonon eigenvectors
Equations	Eq. 1.12 1.15	Eq. 1.12 1.17	Eq. 1.1
Comments	Requires fitting parameters	Require harmonic lattice dynamics and Lorentzian fitting	Requires harmonic lattice dynamics

1.5 Thermal Conductivity Calculation of Periodic Materials

This session reviews literature papers for thermal conductivity in related nanomaterials: superlattices and phononic crystals.

1.5.1 Superlattices

Superlattices are important materials in the phonon transport field because of their unique thermal properties which have been extensively studied. Garg (Garg et al. 2011) used first principle and iterative method to study the thermal conductivity of superlattice with perfect interfaces in a short-period limit, and they found that the thermal conductivity of the superlattice can exceed that of the bulk material and varying the mass mismatch could reduce the thermal conductivity. In a later study for superlattices with rough interfaces, Garg (Garg & Chen 2013) showed that the decrease in the group velocity of low frequency phonons and the interface-disorder-induced scattering of high frequency phonons drive the superlattice thermal conductivity to below the alloy limit. He also found that the interplay between reduced group velocity and an increase in lifetime leads to the minimum thermal condutivity. Increasing the mass-mismatch could further lower the thermal conductivity of superlattices. Huberman (Huberman et al. 2013) studied the disruption of superlattice phonons by interfacial mixing using GKMD, lattice dynamics based BTE methods and showed that both methods agreed for cross-plane k and highlighted the importance of including secondary periodicity. Mizuno (Mizuno et al. 2015) used equilibrium MD method to study the thermal conductivity of layered superlattices and showed that those materials with different mass-mismatch or weakened interactions result in lower thermal conductivity.

1.5.2 Phononic Crystals

Computational modeling offers great potential to engineer the structures of nano-phononic crystals and superlattices to minimize thermal conductivity. Because of its simplicity and minimum computational effort, one of the analytical models, the Callaway-Holland model, has been extensively used to calculate the thermal conductivity for nano-phononic crystals (Gillet et al. 2009, Hopkins et al. 2010, Reinke et al. 2011, El-Kady et al. 2012, Alaie et al. 2015, Davis & Hussein 2014).

The thermal conductivity of nano-phononic crystals have been studied using multiple methods. Callaway-Holland model under isotropic assumption is the most common one. The Callaway-Holland model has been used in different materials, including silicon thin films with multiple air cylinders (Alaie et al. 2015), the silicon nano-phononic crystals with square holes (Dechaumphai & Chen 2012), and the pillar-based nano-phononic crystals (Davis & Hussein 2014). Molecular dynamics has also been used to study the thermal conductivity of nano-phononic crystals. The thermal conductivity of nanoscale Si pillar-on-plate PnCs were studied using molecular dynamics (Honarvar et al. 2016) to investigate the effects of different geometry parameter such as nano-pillar in reducing the thermal conductivity of the base membrane, and found that the thermal conductivity reduction increases as the volume fraction of nano-pillar increases. Molecular dynamics was also used to study the thermal conductivity of a nanoscale three-dimensional (3D) Si phononic crystal with spherical pores (Yang et al. 2014) and found that the thermal conductivity was reduced by a factor of 10,000 times compared to bulk Si at room temperature, and the result depends on the porosity.

1.6 Thermal Conductivity Calculation in Nano-Phononic Crystals: Problems and Assumptions

Even though the Callaway-Holland-based thermal conductivity method has shown good agreement with experimental results in certain situations, questions still remain

with the Callaway-Holland model. We have summarized three major problems with the Callaway-Holland model. The first one is significant errors from the Callaway-Holland model. This model produced up to 25% error in the thermal conductivity calculation for silicon thin film under the isotropic assumption (Sellan et al. 2010). The second problem is inconsistent results. The thermal conductivity for bulk Si using the Callaway-Holland model under the isotropic assumption was decreasing as the simulation supercell size increases (Davis & Hussein 2011), which is not physically meaningful. The last problem is adjusting thermal conductivity results using random geometric parameters, for example, the thermal conductivity of Si/Ge quantum dot phononic crystals were adjusted by a non-dimensional geometric factor f_k = 2 using the Callaway-Holland model (Gillet et al. 2009).

Even though it has been widely used, the Callaway-Holland model is questionable for nano-phononic crystals because there are three major assumptions embedded in it: the isotropic thermal conductivity assumption, the empirical scattering rates assumption, and the effective material assumption. The three assumptions were rooted in the desire to develop a simple analytical model to calculate thermal conductivity for bulk materials; more detailed information can be found in Section 1.3. Those three assumptions may be inappropriate in the thermal conductivity calculation for nano-phononic crystals since they have significant difference in material components and supercell sizes compared to the bulk materials.

First, it has been assumed that the dispersion curves in every directions are same as one of the high-symmetry direction, usually the [100] direction, which results in the isotropic thermal conductivity. This assumption produced good results for bulk materials when using primitive cells, which is the smallest possible unit cell of a lattice, because the the phonons along the [100] direction are representative of the full Brillouin-zone data at low-frequencies and the bulk thermal conductivity is dominated by low frequency phonons (Sellan et al. 2010). However, the authors (Sellan et al. 2010) have shown that the isotropic assumption produces up to 25% error within thin films. This dissertation will examine the validity of the isotropic assumption in nano-phononic crystals.

Second, the Callaway-Holland thermal conductivity calculations in the literature have also used empirical scattering rates based on empirical parameters fit to bulk materials. Since the nano-phononic crystals have multiple materials and much more complicated structures, doubt arises as to the validity of using the same empirical scattering rates from bulk materials in the nano-phononic crystals.

Third, another question associated with nano-phononic crystals is the accuracy of the effective material assumption. In particular, it is not clear whether the effective material assumption in the Callaway-Holland model can correctly calculate or include the properties for phonons with wavelength in the same scale or shorter than the supercell size. When the supercell increases as the periodicity of a nano-phononic crystal increases, there are more portions of phonons with wavelength in the same scale or shorter than the supercell size. The effective material assumption is appropriate for phonons with wavelength much longer than supercell size, however, it may incorrectly calculate the phonons with wavelength shorter than the supercell size or incorrectly calculate the properties for those phonons, which will be explained in Section 4.

More information on those assumptions can also be found in Chapters 2 to 4.

1.7 Goals

In summary, the validity of the following assumptions associated with the isotropic Callaway-Holland model will be examined in this dissertation:

1. The isotropic thermal conductivity assumption in supercell lattice dynamics calculation;

2. The assumption that empirical scattering rates derived from bulk materials can be used for nano-phononic crystal calculations;

3. The effective material assumption in nano-phononic crystals.

Chapter 2

Examination of the Isotropic Thermal Conductivity Assumption for Nano-Phononic Crystals

2.1 Literature Reviews on Isotropic Assumption

As discussed before, thermal conductivity can be calculated by solving the full Boltzmann Transport Equation (BTE), which is tedious (Chen 2005). A simpler method, derived from the BTE and expressed in terms of relaxation time, has been presented by Klemens (Klemens 1958). In its most general form, this expression involves a direct summation of the heat current contributions of individual phonons of all wavevectors and polarizations in the first Brillouin zone, called the direct summation method in this paper.

In common practice, the direct summation expression is simplified by making an isotropic assumption that converts the summation over wavevector to an integral over wavevector magnitude. This approach, proposed by Callaway (Callaway 1959) and Holland (Holland 1963), yields calculated thermal conductivities that agree well with experimental data on many bulk materials, for example Si and Ge (Slack & Glassbrenner 1960, Glassbrenner & Slack 1964). Because of its simplicity and mini-

mal computation effort, the Callaway-Holland approach, referred to as the "isotropic method" for the remainder of this paper, has been used to predict the thermal conductivity of various nanomaterials including Si and Ge nanowires (Mingo et al. 2003), Si/Ge quantum dot superlattices (QDSL) (Gillet et al. 2009), periodic microporous (Hopkins et al. 2009) and nanomesh (Alaie et al. 2015) membranes, Si/nanovoid superlattices (Davis & Hussein 2011), nanoscale phononic crystal slabs (Reinke et al. 2011), porous silicon nanobridges (Marconnet et al. 2012), pillared silicon thin films (Davis & Hussein 2014), and two-side branched nanowires (Li et al. 2017). While one study reports that a partial coherence approach based on the isotropic method agrees well with phononic crystal experimental data (Dechaumphai & Chen 2012), others raise issues for further exploration with respect to the applicability of the isotropic method for phononic crystal and superlattice calculations. These include the origin of the decrease of bulk Si thermal conductivity with increasing supercell size (Davis & Hussein 2011) and the ability of a single geometric factor to appropriately adjust the isotropic thermal conductivity results to account for non-spherical Brillouin zones (Gillet et al. 2009). Even though it has been shown that the isotropic assumption becomes increasingly less accurate compared to the full Brillouin-zone method as the silicon film thickness is reduced (Sellan et al. 2010), the reason behind the discrepancy is not clear. Meanwhile, the validity of the isotropic method has not been carefully evaluated for superlattices and phononic crystals of different periods or supercell sizes. With the recent surge of interest in predicting the thermal properties of phononic crystals, such evaluation becomes increasingly important. One of the easiest ways to evaluate the isotropic method is to compare it with the direct summation method, which has been successfully applied to different nanomaterials, including Si and Ge (Klemens 1958), and Si/Ge and GaAs/AlAs superlattices (Tamura et al. 1999, Yang & Chen 2003).

2.2 Methods to Validate the Assumption

In this section, the thermal conductivities of different materials, including bulk Si, and Si/Ge QDSLs are calculated using the direct summation and isotropic models. Key inputs to the models are group velocities, which are obtained from dispersion relations generated with harmonic lattice dynamics calculations (Dove 1993), and relaxation times, which are computed using established empirical equation models (Gillet et al. 2009, Glassbrenner & Slack 1964, Davis & Hussein 2011). Calculations were performed for various different sized supercells, which are the periodically repeating building blocks used to generate phononic crystal structure.

To examine the validity of the isotropic assumption further, we compared the results of direct summation and isotropic calculations on various QDSL configurations. Si/Ge QDSLs with supercell side length varying from two to five CCs of Si and a single CC of Ge in the center, as seen in Fig. 2.1, were investigated first. Ge/Si QDSLs with the same geometry as the Si/Ge systems but with reversed atom positions were also investigated in order to explore the effects of material configuration on thermal conductivity.

2.2.1 Theory and Methods

The lattice thermal conductivity computed using the direct summation method, k_{FBZ}, is given by (Klemens 1958)

$$k_{FBZ} = \sum_{\lambda} C_{ph}(\vec{q},\lambda) v^2(\vec{q},\lambda) \tau(\vec{q},\lambda) \tag{2.1}$$

where C_{ph}, $\vec{q}$, v, and τ are specific heat, wavevector, component of phonon group velocity in the direction of interest, and the phonon relaxation time. λ specifies both the phonon wavevector and frequency. The summation is taken over all phonons in the full Brillouin zone, as noted by the subscript FBZ. The specific heat is given as $C_{ph}(\vec{q},\lambda) = k_B x^2 \exp(x)/(\exp(x)-1)^2$, where $x = \hbar\omega(\vec{q},\lambda)/k_B T$ and k_B, $\hbar$, T, and ω are Boltzmann's constant, reduced Planck's constant, temperature, and angular

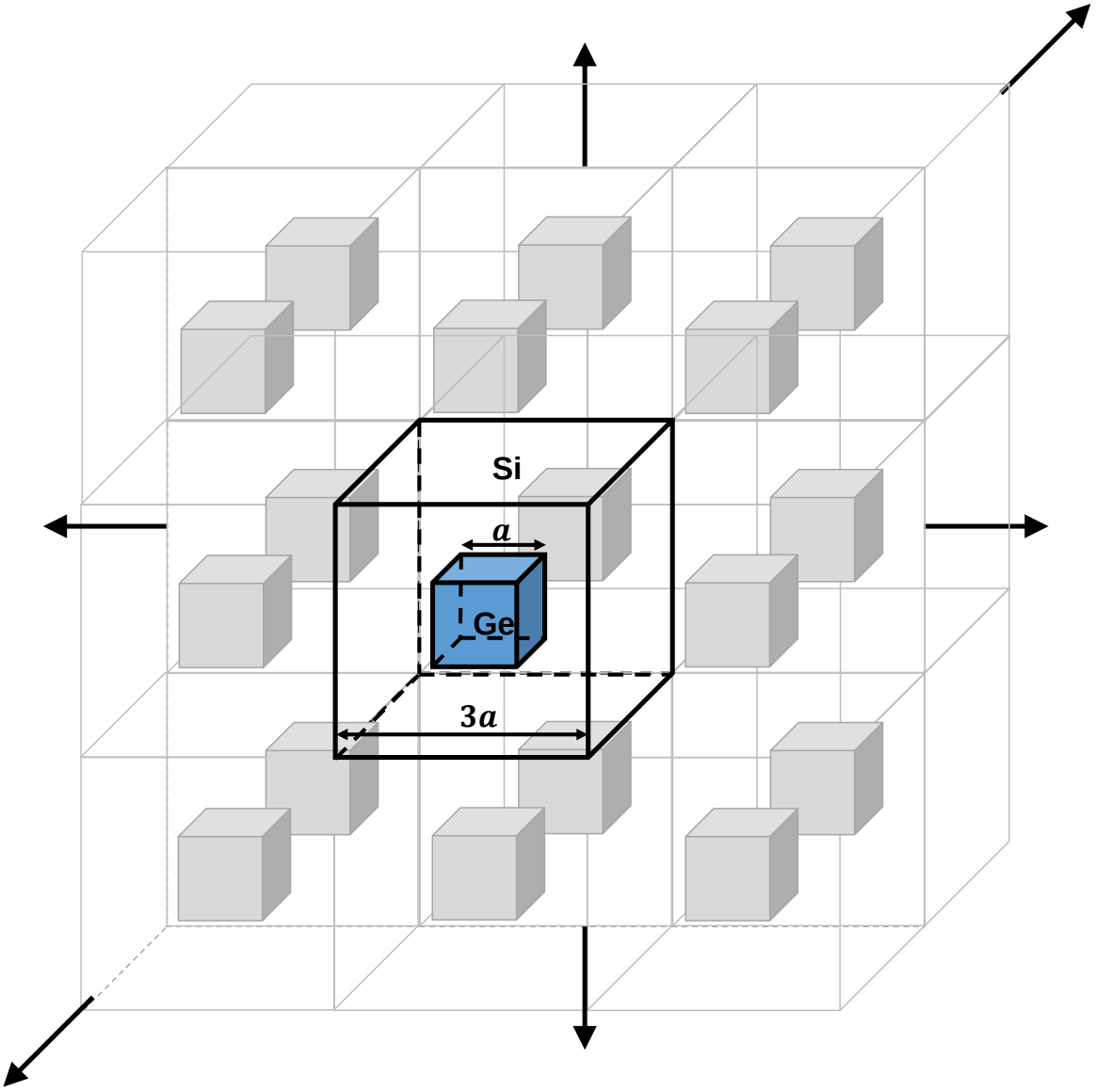

Figure 2.1: Schematic of Si3Ge1 quantum dot superlattice. The silicon supercell is the central cube with black boundaries. It has a side length of 3 CCs and is embedded with a blue germanium quantum dot with side length 1 CC. The supercell is repeated infinitely in all directions, as indicated by the neighboring "image" supercells with faint gray quantum dots.

frequency. In the isotropic assumption, Eq.(1) is converted to (Holland 1963)

$$k_{ISO} = \frac{1}{6\pi^2} \int_{q=0}^{q_{max}} C_{ph}(q,\lambda) v^2(q,\lambda) \tau(q,\lambda) q^2 dq \tag{2.2}$$

where q is the wavevector magnitude in a chosen direction. The group velocity is calculated using $\vec{v} = \frac{\partial \omega}{\partial \vec{q}}$, where the dispersion relation $\omega(q)$ is obtained from atomistic lattice dynamics calculations (Zhao & Freund 2005). Since thermal conductivities in the [100] and [110] directions are considered in this paper, $v = \frac{d\omega}{dq}$ is used to calculate group velocity in each direction respectively. The derivative is evaluated numerically for each phonon with wavevector q by applying small perturbations $+/-dq$ in that direction, calculating the frequencies at $q+dq$ and $q-dq$, and dividing their difference $d\omega(\lambda)$ by $2dq$. It was found that the value of group velocity was independent of the perturbation magnitude for $dq < 0.6e-3rad/nm$, so perturbations at or below this value were used for all group velocity calculations. A significant numerical challenge in calculating group velocities for materials with complex dispersion relations is to make sure that the frequencies $\omega(q+dq)$ and $\omega(q-dq)$ are evaluated on the same phonon branch (λ). Recognizing that the eigenvectors of two phonon modes on the same branch point in the same direction when these modes have infinitesimally different q values, we verified that the eigenvectors were parallel before proceeding with group velocity calculations. Branch-dependent group velocity results can be found in Fig. A.1 of the Appendix. A linearized Stillinger-Weber potential was used in this study and all the parameters used in this work can be found in Ref. (Zhao & Freund 2005).

In general τ depends on phonon-phonon, phonon-boundary, and phonon-defect scattering (Klemens 1958). In QDSL, it additionally depends on phonon-nanoparticle scattering (Kim & Majumdar 2006, Gillet et al. 2009). In this section, the relaxation time for bulk Si is expressed as $\tau = [\tau_U^{-1} + \tau_I^{-1}]^{-1}$, where $\tau_U^{-1} = BT\omega^2 \exp(-C/T)$ represents Umklapp phonon-phonon scattering and $\tau_I^{-1} = D\omega^4$ represents defect scattering by impurities. The relaxation time for Si/Ge and Ge/Si QDSL is expressed as $\tau = [\tau_U^{-1}+\tau_{NP}^{-1}+\tau_I^{-1}]^{-1}$, where $\tau_{NP}^{-1} = \eta v\left((\sigma^f)^{-1}+(\sigma^n)^{-1}\right)^{-1}$ represents nanoparticle scattering with $\sigma^f = \pi R^2\chi^4 h_1(\chi, \Delta M/M, \Delta K/K)$ and $\sigma^n = 2\pi R^2 h_2(\chi, \Delta M/M, \Delta K/K)$. Here η, M, and K are the nanoparticle volumetric density, the mass of the host medium, and force constant of the host medium, and $\chi = qR$ is the size parameter for a scatterer with the characteristic radius $R = a/2$ in this paper. For both QDSL types, the parameter B in τ_U is taken from the host material's value while the angu-

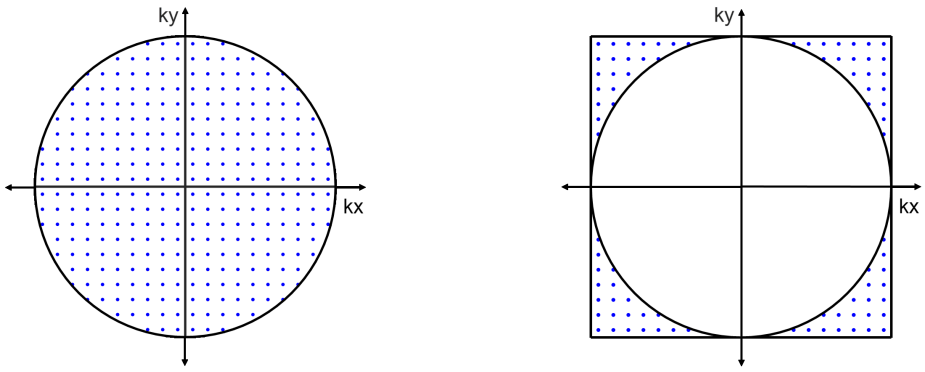

(a) (b)

Figure 2.2: (a) Spherical Brillouin zone and (b) Neglected phonons.

lar frequency is taken from actual dispersion curves. Detailed information about the functions, h_1, and h_2, can be found in Refs. (Kim & Majumdar 2006, Gillet et al. 2009). The values of the parameters used in the relaxation time calculations (Table 3.1) are taken from Refs. (Singh et al. 2011, Gillet et al. 2009).

Table 2.1: Simulation parameters

	B(sK^{-1})	C(K)	D(s^3)	$\Delta M/M$	$\Delta K/K$
Si	$1.73e-19$	137.39	$1.32e-45$	1.5849	0.2410
Ge	$3.35e-19$	57.6	$2.40e-44$	−0.6131	−0.3175

2.3 Results

The thermal conductivity predictions from the isotropic and direct summation methods in various materials with different supercell sizes will be presented in this section. We first verify the simulation code by comparing the results in this work to literature papers, we then calculate the thermal conductivity results in bulk Si, Si/Ge QDSLs, and Ge/Si QDSLs.

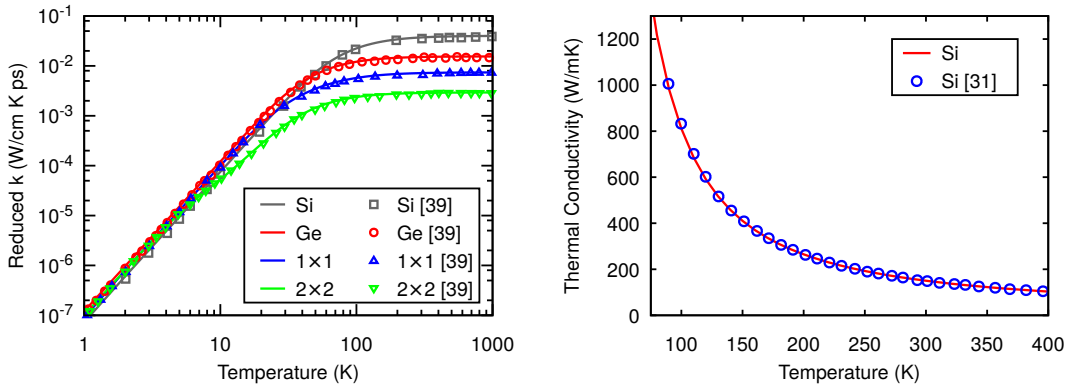

(a) (b)

Figure 2.3: (a) Reduced thermal conductivity for Si, Ge and Si/Ge superlattices with different periodicity; (b) Thermal conductivity for bulk Si. Lines are results from this work, markers in (a) are results from Ref. (Tamura et al. 1999), and markers in (b) are results from Ref. (Hopkins et al. 2009).

2.3.1 Verification of Modeling Methods

Before examining the validity of the isotropic assumption, we first verified the direct summation and isotropic methods against benchmark data in the literature. The direct summation results were compared to the reduced thermal conductivity data computed by Tamura *et al.* (Tamura et al. 1999) for bulk Si, bulk Ge, and Si/Ge superlattices with different atom layer thicknesses as shown in Fig. 2.3 (a). In Fig. 2.3 (a), the superlattice unit cell geometry is denoted $n \times m$, where n and m refer to the thicknesses of the Si and Ge layers, respectively, in terms of the number of atomic layers in the superlattice unit cell. Using the same potentials, geometries, and lattice constants, we obtained very good agreement with Tamura's results. Additionally, we compared our isotropic method thermal conductivity calculations to those of Hopkins *et al.* (Hopkins et al. 2009) for bulk Si. Excellent agreement between the two is found (Fig. 2.3 (b)).

2.3.2 Bulk Silicon

After verifying our method, the thermal conductivity of bulk Si with different supercell sizes was calculated using both direct summation and isotropic methods. Convergence

tests with different q-space resolution show that the thermal conductivities achieve stability for q-space intervals d_q below 0.025 rad/nm, so the value 0.025 rad/nm was used for all calculations. Figure 2.4 shows that the direct summation method gives a constant thermal conductivity for all supercell sizes, as expected. In contrast, the isotropic thermal conductivity results decrease with supercell size, showing a similar trend to that observed in Ref. (Davis & Hussein 2011). The decreasing behavior predicted from the isotropic method is not physically meaningful, as the choice of supercell size should not affect the thermal conductivity of a bulk material. Moreover, the difference between the direct summation and the isotropic methods for bulk Si increases as the supercell size increases. This implies that the isotropic method is increasingly unreliable for predicting thermal conductivities when the supercell size increases and indicates that great care must be taken when using it to predict the thermal conductivity of supercell-based systems such as superlattices, nano phononic crystals, and other periodic structures.

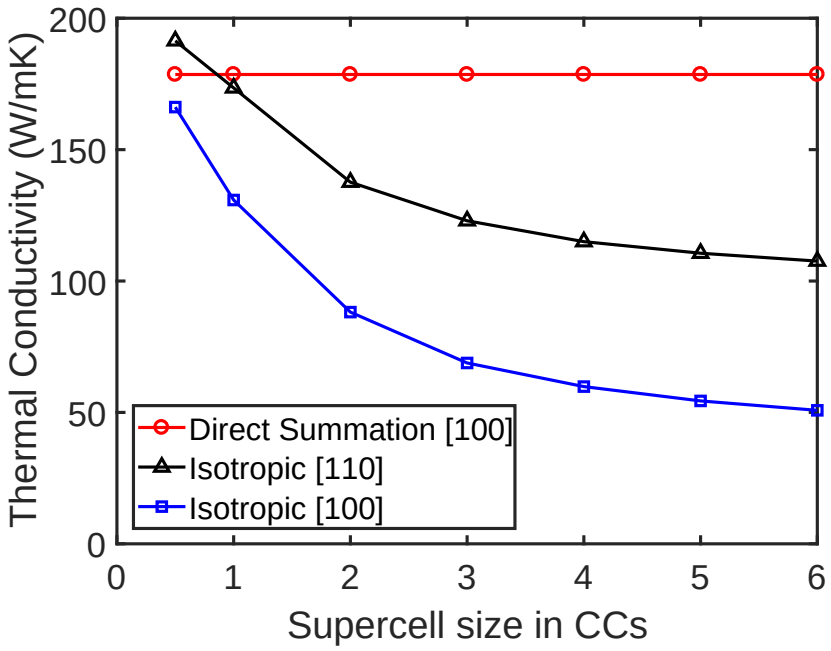

Figure 2.4: Thermal conductivity of bulk Si with different supercell sizes using the direct summation and isotropic methods.

2.3.3 Silicon/Germanium Quantum Dot Superlattices

To examine the validity of the isotropic assumption further, we compared the results of direct summation and isotropic calculations on various quantum dot superlattices (QDSL) configurations. Si/Ge QDSLs with supercell side length varying from two to five CCs of Si and a single CC of Ge in the center, as seen in Fig. 2.1, were investigated first. Ge/Si QDSLs with the same geometry as the Si/Ge systems but with reversed atom positions were also investigated in order to explore the effects of material configuration on thermal conductivity. The thermal conductivity results for Si/Ge, Ge/Si QDSLs in the [100] direction, and Si/Ge QDSLs in the [110] direction are shown in Fig. 2.5 (a), (b), (c), respectively. For both methods and in both QDSL types, the thermal conductivity increases toward the bulk value of the host material as the supercell size increases. This increase occurs because the nano particle relaxation time decreases relative to the Umklapp and impurity relaxation time as supercell size increases, leading to longer phonon lifetimes and higher thermal conductivities. It is also observed that the Si/Ge QDSL thermal conductivity increases at a higher rate than that of the Ge/Si QDSL. This is thought to occur because the increase in volume fraction of host material with supercell size is another factor, in addition to the decrease in phonon-nanoparticle relaxation time, that impacts thermal conductivity. In the Si/Ge QDSL case, the host material (Si) thermal conductivity is higher than that of the QD (Ge). This leads to thermal conductivity enhancement beyond that determined by nanoparticle scattering alone. In contrast, the lower thermal conductivity of the Ge host material in Ge/Si QDSL leads to a suppression of overall thermal conductivity below that determined by nanoparticle scattering alone. This suppression is not strong enough to offset the increase with supercell size due to reduction in nanoparticle relaxation time, so the Ge/Si QDSL thermal conductivity follows the same trend as that of Si/Ge QDSL. More interestingly, the thermal conductivities from direct summation grow more rapidly with supercell size than those from the isotropic method. This is similar to the case of bulk Si, where the isotropic thermal conductivity deviates more strongly from the direct summation results as supercell

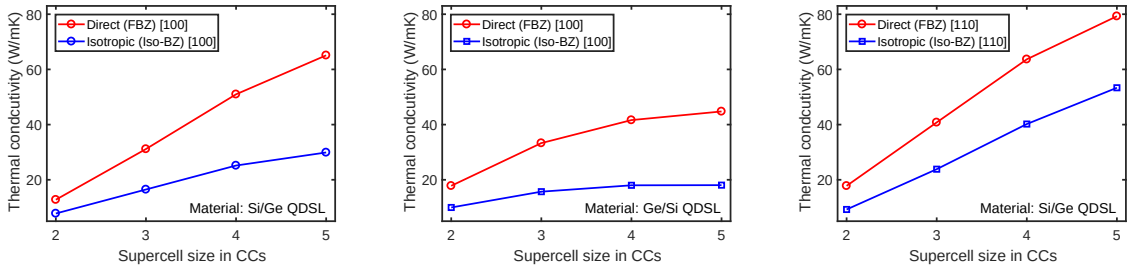

Figure 2.5: Thermal conductivity of (a) Si/Ge QDSLs in [100] direction, (b) Ge/Si QDSLs in [100] direction and (c) Si/Ge QDSLs in [110] direction.

size increases.

The difference between the isotropic assumption and the direct summation methods can be more clearly quantified by calculating the ratio of k_{ISO} (Eq. 1.15) and k_{FBZ} (Eq. 1.12), as shown in Fig. 2.6 for Si/Ge QDSL, Ge/Si QDSL, and bulk Si in the [100] direction. For all three cases, the isotropic thermal conductivity results drift further away from the direct summation results as the supercell size increases. The change of the ratio from the smallest supercell to the largest supercell is 15% to 25% in all three cases.

2.4 Discussion

Despite the differences in supercell configurations and materials studied, all of the previous results show that isotropic calculations underpredict thermal conductivity when compared to the direct summation case, and that this effect becomes more pronounced for larger unit cell materials. There are two possible reasons for the differences between k_{ISO} and k_{FBZ}: 1) the effects of crystal anisotropy, which are not considered in the isotropic model, and 2) the effects arising from Brillouin zone geometry, which is different for the isotropic and direct summation models. We examine these two effects by constructing an artificial spherical Brillouin zone (SBZ), computing its thermal conductivity k_{SBZ} using Eq. (1), and comparing the results separately to the Iso-BZ and FBZ results. Like the FBZ thermal conductivity calculation, the

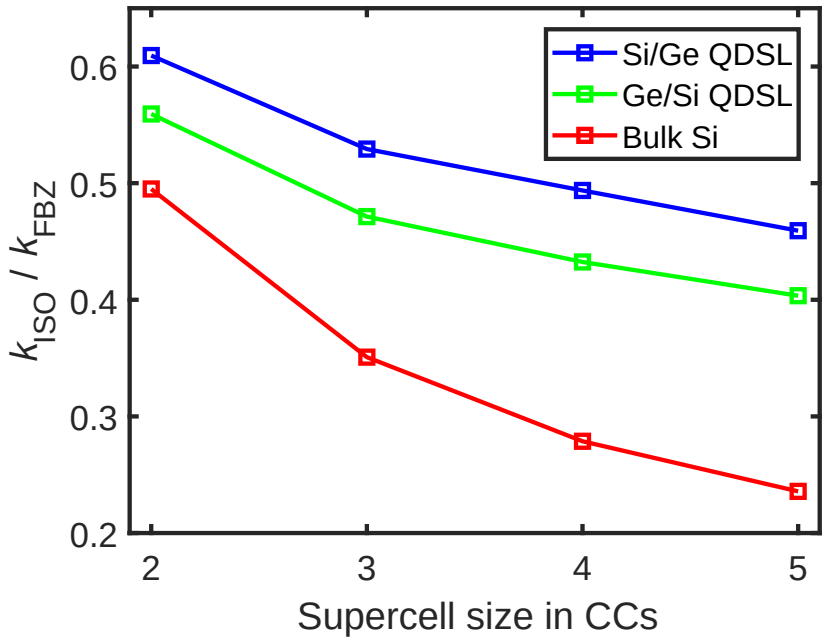

Figure 2.6: Ratio of the isotropic and direct summation results in bulk Si, Si/Ge QDSLs, and Ge/Si QDSLs along the [100] direction.

SBZ calculation uses the exact dispersion curves to sum the thermal conductivity contributions at each wavevector inside the Brillouin zone. Unlike the FBZ calculation, the SBZ only includes points within the sphere defined by the [100] zone edge (Fig. 2.2 (a)). The wavevectors in the space between the SBZ and FBZ edges are denoted "neglected phonons" (Fig. 2.2 (b)). The SBZ and the Iso-BZ calculations share the same zone edge, but differ in that the Iso-BZ calculations are isotropic and only consider dispersion data in the [100] direction.

The effect of anisotropy is analyzed first, by computing the ratio $(k_{SBZ}-k_{ISO})/k_{FBZ}$ for Si/Ge and Ge/Si QDSLs. This ratio represents how much the isotropic thermal conductivity, computed using dispersion data in a high symmetry [100] direction, is lower than the direct summation thermal conductivity computed in a Brillouin zone of the same size and shape. Figure 2.7 shows, for both types of QDSLs, that the anisotropy effect contributes less than 23% to the overall FBZ thermal conductivity and that there is only a small dependence on supercell size.

Next, the effect of Brillouin zone geometry is analyzed, by computing the ratio

$(k_{FBZ}-k_{SBZ})/k_{FBZ}$ for the QDSLs. This ratio represents the fraction of total thermal conductivity that is contributed by neglected phonons outside the SBZ. The ratio of the number of neglected phonons to the number of FBZ phonons depends only on the ratio of spherical and full Brillouin zone volumes, and thus is constant with respect to supercell size. This is evident from Fig. 2.8, which shows as shaded areas the reciprocal space volumes neglected for $2 \times 2 \times 2$ and $4 \times 4 \times 4$ supercells. Figure 2.8 also shows how the real space representations and the Brillouin zones differ for these supercells.

It is not known whether the ratio of thermal conductivities will also be constant with supercell size. If so, a simple thermal conductivity scaling approach based on the ratio of Brillouin zone volumes is appropriate to estimate thermal conductivity (Ref. (Gillet et al. 2009)). Figure 2.7, however, shows that the thermal conductivity ratio for the various QDSLs is not constant. The increasing trend for $(k_{FBZ}-k_{SBZ})/k_{FBZ}$ indicates that the phonons outside the SBZ contribute more to thermal conductivity as supercell size increases and that the neglected phonon contribution becomes more important.

To understand why the neglected phonons become increasingly important for larger supercells, C_{ph}, v^2, τ, k, and $1/\omega^2$ are averaged for the neglected phonons in the [110] direction and for all phonons in this direction, and their ratio is taken for bulk Si. This direction is chosen because it contains a significant number of neglected phonons, as illustrated in Fig. 2.8. Figure 2.9 (a) shows that the ratios for C_{ph} and v^2 are very close to one, which means that these parameters do not have any significant effect on the thermal conductivity supercell size dependence. The trends for τ and k are the same, indicating that the relaxation time is the primary reason for the difference. This behavior for τ arises from umklapp scattering, which has $1/\omega^2$ dependency and is shown in Fig. 2.9 (a). To examine the sensitivity of this result with respect to τ, three different expressions for τ are used to compute the thermal conductivity of bulk Si. Since umklapp scattering is dominant in bulk Si, the main difference in these three expressions is the coefficient for the umklapp relaxation time, whose form varies from $B\omega^2 T \exp(-C/T)$ (Davis & Hussein 2011) to $B\omega^2/\sinh(x)$

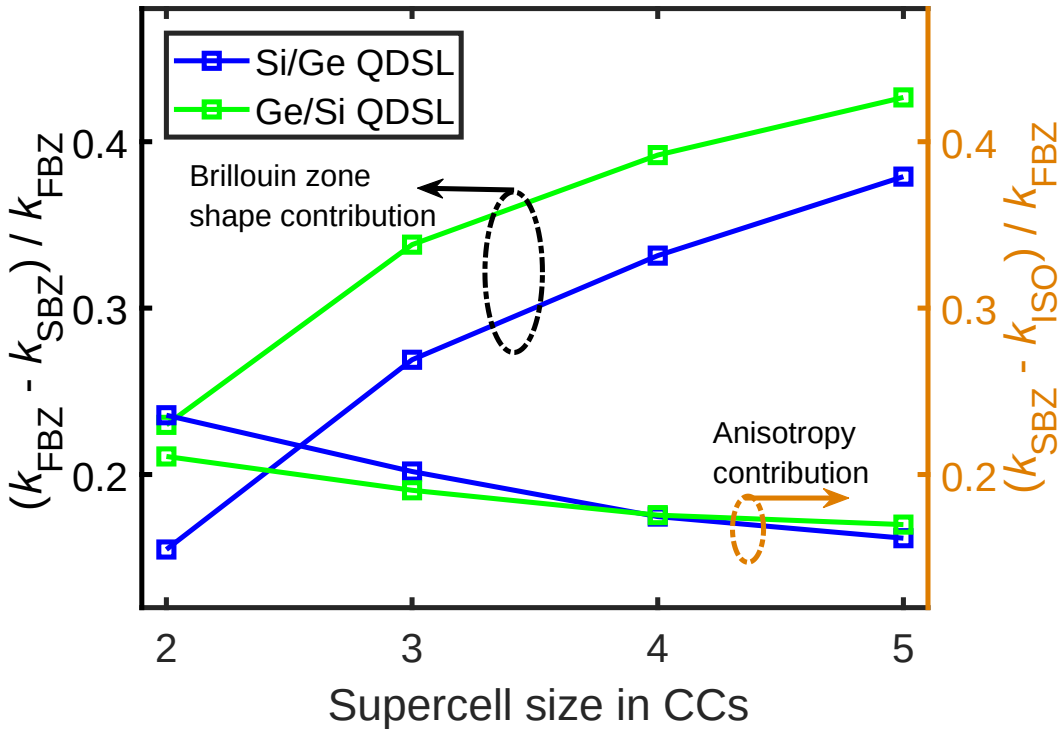

Figure 2.7: Ratios of the Brillouin shape effect ($k_{FBZ}-k_{SBZ}$) and the anisotropic effect ($k_{SBZ}-k_{ISO}$) to the direct summation result (k_{FBZ}) in Si/Ge and Ge/Si QDSLs along the [100] direction.

(Holland 1963) and $B\omega^2/v^2$ (Gillet et al. 2009). Even though the ratio of k_{ISO}/k_{FBZ} depends on τ, Fig. 2.9 (b) shows that the trends of this ratio are similar for all three cases. There are some limitations in the above relaxation time assumptions (Ward & Broido 2010). First of all, the relaxation times due to phonon-phonon scattering were originally developed for small phonon frequencies and low temperatures where the resistive umklapp scattering processes are weak. Second, the constants in these equations are usually determined by fitting to experimental data. Regardless of the particular form chosen for τ, it is clear that the increase in τ of the neglected phonons is responsible for the decrease of k_{ISO}/k_{SBZ} with supercell size.

To better understand why the average τ of neglected phonons increases with supercell size, the branch averaged τ at each q point, denoted $\langle\tau(q)\rangle$, is calculated at each point along the [110] direction. Each $\langle\tau(q)\rangle$ is then normalized by the branch- and q- averaged relaxation times ($\frac{1}{n_q}\sum_q\langle\tau(q)\rangle$). The normalized branch averaged $\langle\tau(q)\rangle$,

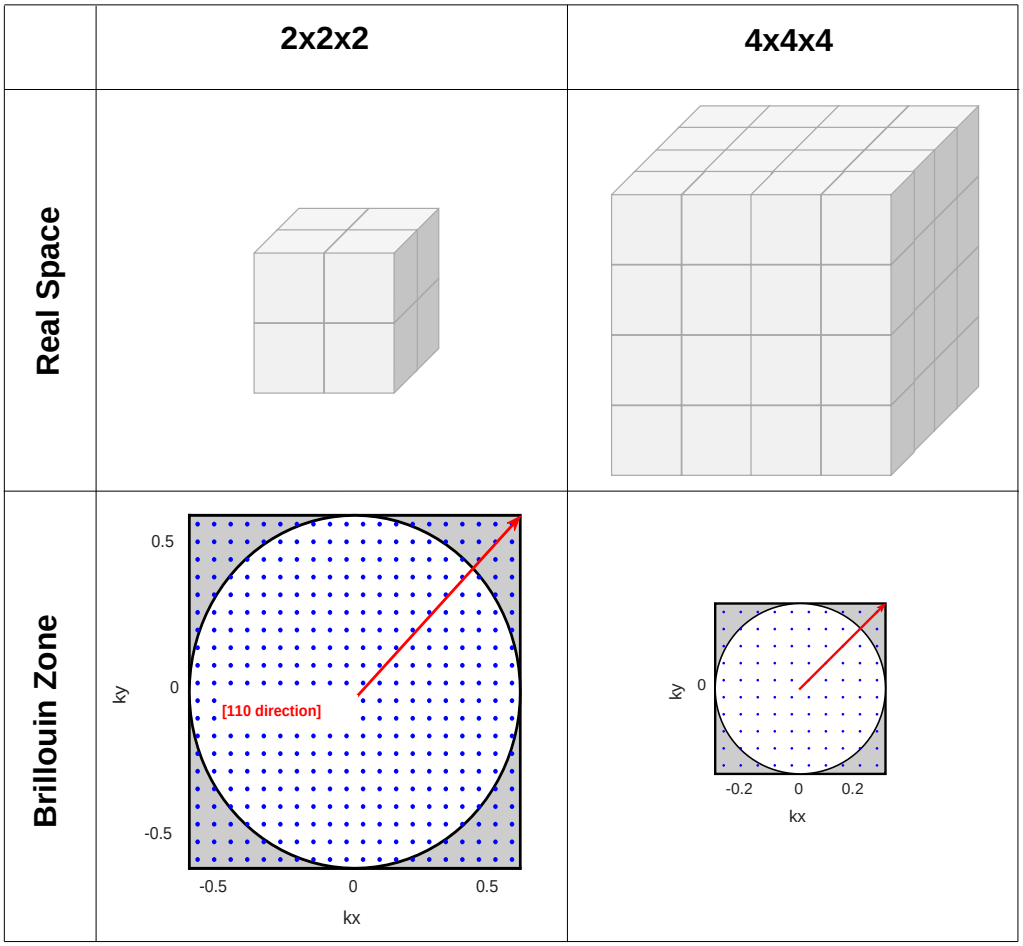

Figure 2.8: Real space representations and Brillouin zones for supercell with (a) $2 \times 2 \times 2$ CCs and (b) $4 \times 4 \times 4$ CCs.

$n_q \langle \tau(q) \rangle (\sum_q \langle \tau(q) \rangle)^{-1}$, is plotted in Fig. 2.10 for bulk Si with different supercell sizes. For all supercell sizes, the smallest wavevector phonons have the longest relaxation times. As wavevector increases, relaxation times decrease monotonically to asymptotic values that are highest for the largest supercells. Since the normalized $\langle \tau(q) \rangle$ of the neglected phonons in the largest supercells is bigger, relative to $\frac{1}{n_q} \sum_q \langle \tau(q) \rangle$, than that of the smaller supercells, these neglected phonons provide a higher contribution to thermal transport. Thus, as supercell size increases, the isotropic assumption underpredicts thermal conductivity more strongly. Another interpretation of these results: because the extent of the Brillouin zone decreases as supercell size increases (Fig. 2.8), the neglected wavevectors are smaller, and thus their lifetimes and thermal

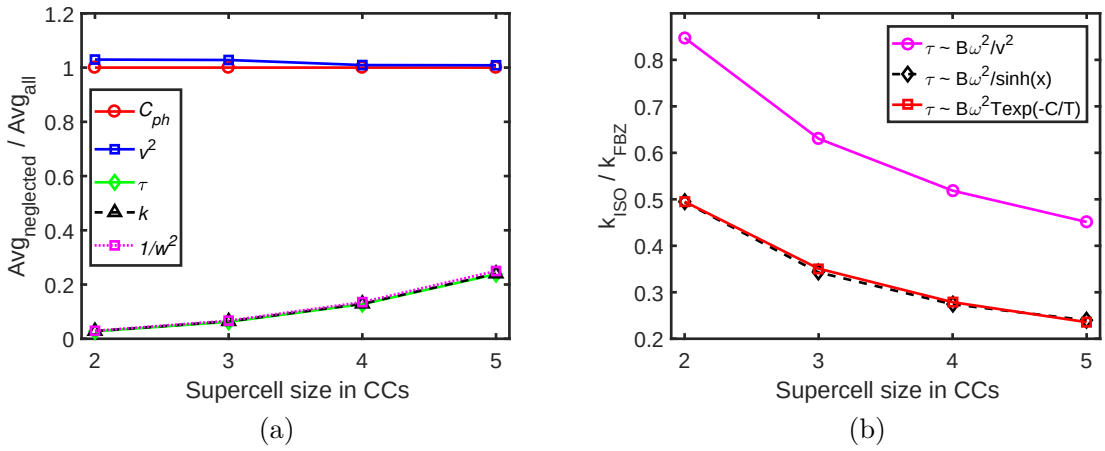

Figure 2.9: (a) Ratio of average value from neglected and all phonons in [110] direction in bulk Si, and (b) ratio of isotropic assumption result to full Brillouin zone result in bulk Si using three different τ expressions.

conductivity contribution are larger.

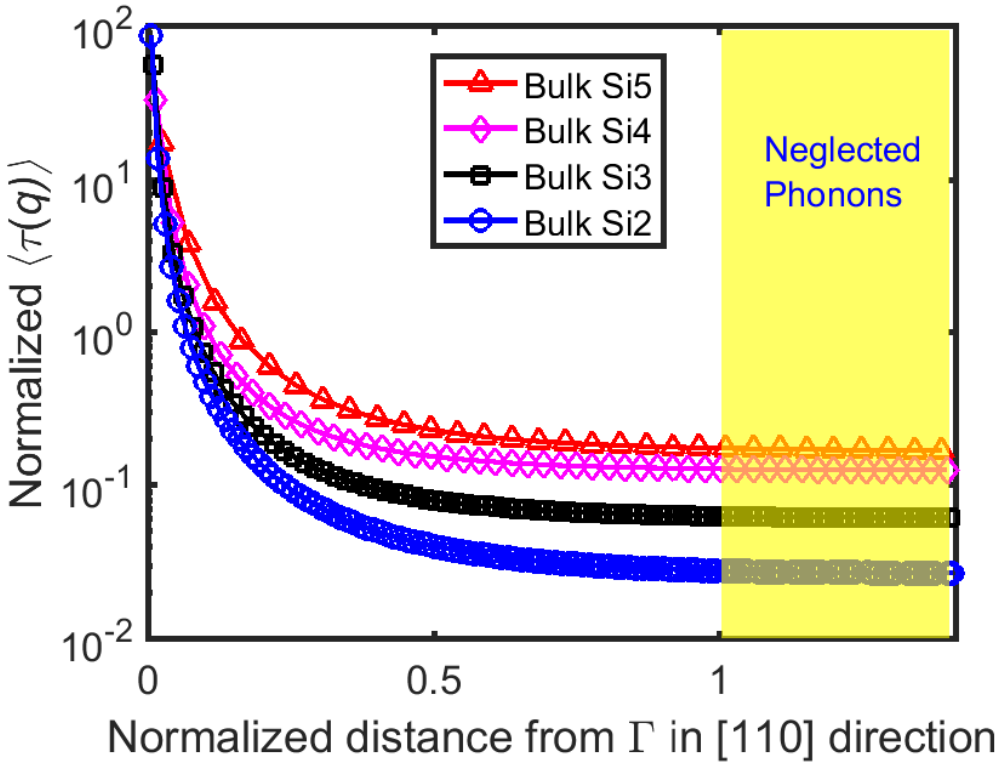

Figure 2.10: Normalized branch averaged $\langle \tau(q) \rangle$ in [110] direction for different bulk silicon supercell sizes.

Finally, the overall contribution to thermal conductivity from neglected phonons in all directions is computed as a function of supercell size (Fig. 2.11). A notable increase from the 15% – 23% range to the 37% – 43% range is observed for Si/Ge and Ge/Si QDSLs as supercell size increases. These results indicate that the phonons neglected in SBZ calculations provide a significant contribution to thermal conductivity and should not be neglected.

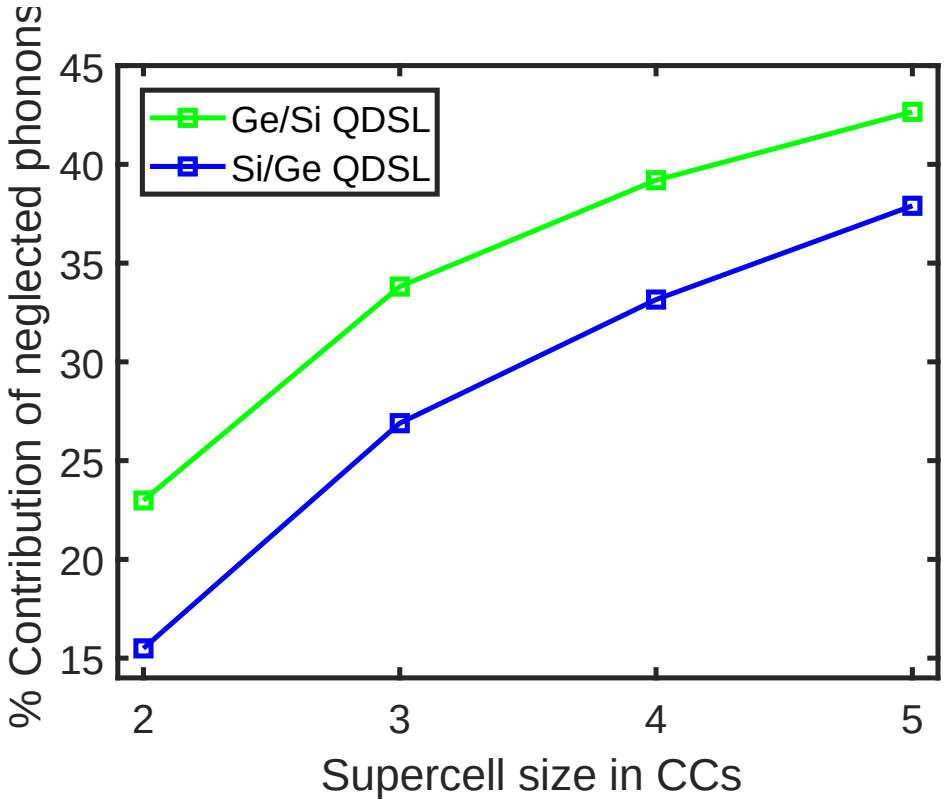

Figure 2.11: Percentage contribution of neglected phonons to thermal conductivity in Si/Ge and Ge/Si QDSLs along the [100] direction.

2.5 Conclusions

In summary, the direct summation method yields the same bulk Si thermal conductivity value with different supercell sizes, which is physically meaningful and comparable with results from other works. The difference between the direct summation and isotropic methods depends substantially on the supercell size for both bulk Si and Si/Ge quantum dot superlattices. The thermal conductivity contribution

from phonons neglected in the isotropic assumption calculations increases as supercell size increases, which can be explained by the increased relaxation time of neglected phonons. While significantly smaller than the effect of Brillouin zone shape, the effect of crystal anisotropy has a non-negligible contribution to the thermal conductivity dependence on supercell size.

Chapter 3

Examination of the Empirical Relaxation Time Assumption for Nano-Phononic Crystals

In the previous chapter, (Ma & Lukes 2018), we discussed the isotropic assumption models to study Si/Ge quantum dot superlattices (QDSLs). The results indicated that phonon-phonon scattering rates are very important to correctly simulate the thermal conductivity of large supercells. It also implied that the contribution of the phonon-phonon scattering rates are influenced by the supercell size of the nano-phononic crystals and the phonon-phonon scattering rates may be different for different geometries (or roughness). This finding piqued the interest in studying mode-dependent τ in nano-phononic crystals using more accurate methods including the normal mode analysis method, which has not been done before.

As briefly mentioned in the previous sections (section **??**), the relaxation times for each phonon mode are inputs to the Callaway-Holland models (Eq. 1.15) to calculate the thermal conductivity. Methods for obtaining the relaxation time is critical for effective calculations of the thermal conductivity of nano-phononic crystals. This section will first cover empirical scattering equations to calculate τ in both bulk materials and nano-phononic crystals, and then explain the non-empirical methods for τ calculations including first principles and Normal Mode Analysis methods. Finally,

the lifetimes for bulk Ar and Ar/Heavy Ar QDSLs from empirical equations are benchmarked with those values from Normal Mode Analysis.

3.1 Literature Reviews

The mode-dependent phonon-phonon relaxation time is the characteristic time for a system to reach an equilibrium condition after a disturbance, which is τ for each phonon normal mode in Eq. (1.15). The mode dependent phonon-phonon relaxation time is very important for three reasons. First, it provides much more detailed information about phonon transport in the nano-materials. Second, it could give more accurate data to correctly calculate thermal conductivity. Third, it could potentially provide insight on how to manipulate the phonon transport to achieve lower thermal conductivity, specifically which part of phonons contributes the most to thermal transport and which part of phonons should be blocked.

3.1.1 Empirical Relaxation Time Equations

The most straightforward calculation method for relaxation time is the empirical (analytical) models, which is briefly summarized in Table 3.1. T is temperature, subscripts N, U, T, and L indicate the normal scattering, umklapp scattering, transverse and longitudinal wave, respectively; A, B, B_U, B_N and C are constants; θ is Debye temperature; α is a numerical constant. Those empirical equations have been used by various researchers for specific occasions. Even though the results may agree with experimental data, the empirical equations lack the agreement with more accurate methods.

3.1.2 Non-Empirical Relaxation Times

In the last two decades, a few non-empirical methods have been developed to study mode dependent relaxation times including the iterative method with Fermi Golden rule and the normal mode analysis methods. The iterative method with Fermi Golden

Table 3.1: Empirical equations of inverse relaxation time for different scattering processes (adapted from Feng & Ruan (2014))

Scattering process	Empirical equations
Normal process (Three-phonon)	$\tau_N^{-1} = B_N\omega^2T^3$ (Callaway 1959)
Umklapp process (Three-phonon)	$\tau_U^{-1} = B_U\omega T^3 exp(-\frac{\theta}{\alpha T})$, low T (Klemens 1958)
Umklapp process (Three-phonon)	$\tau_U^{-1} = B_U\omega^2T^3$ (Callaway 1959)
Umklapp process (Three-phonon)	$\tau_U^{-1} = \frac{B_{TU}\omega^2}{sinh(x)}, \omega_1 \leq \omega \leq \omega_2$ (Holland 1963)
Boundary	$\tau_{bs}^{-1} = \frac{v_\lambda}{lF}$, $l : diameter$,F : surface roughness (Casimir 1938, Berman & Ziman 1953)
Impurity	$\tau_{imp}^{-1} = \frac{\pi}{2}g\omega^2D(\omega) \sim A\omega^4$ (Klemens 1955)

rule uses the 2nd and 3rd force constants from Ab Initio calculation or classical potential to calculate the scattering rates, has been extensively studied for bulk materials (Broido et al. 2005, Esfarjani & Stokes 2008, Chernatynskiy & Phillpot 2015*b*), and short-period superlattices (Garg et al. 2011, Garg & Chen 2013). The notable results using the Fermi's Golden Rule and iterative method including the phonon relaxation time results in the bulk Si by Broido (Broido et al. 2007) and the relaxation times and phonon thermal properties in Si/Ge superlattice by Garg and et al. (Garg & Chen 2013).

Such spectral dependent information has also been studied using molecular dynamics (MD). For example, McGaughey et al. (McGaughey & Kaviany 2004), Henry et al. (Henry & Chen 2008), Qiu et al. (Qiu et al. 2012), and Feng et al. (Feng & Ruan 2014) used the phonon spectral energy density (SED) or equivalently, time domain normal mode analysis (TDNMA) methods in the framework of equilibrium molecular dynamics (EMD) simulations to extract the spectral dependent scattering rates. In addition, Zhou and Hu (Zhou et al. 2015) developed time domain direct decomposition method (TDDDM) based on nonequilibrium molecular dynamics (NEMD) simulations to study the mode specific phonon-phonon scattering and successfully match the results with SED method for bulk Si and Ar, which is one of the biggest advantages of TDDDM compared to SED and TDNMA in EMD simulations. They also found that those phonon modes with mean free path larger than system sizes are truncated in NEMD. However, papers which used non-empirical scattering rates have

not compared the mode dependent scattering rates to the geometry of the materials. Turney and McGaughey also evaluated the thermal conductivity for Ar and showed that the normal mode analysis (NMA) method was equivalent with other methods such as GKMD (Turney 2009). In this chapter, the normal mode analysis (NMA) method will be used to study the mode dependent lifetimes.

Research Gap

The normal mode analysis method is potentially one of the best tools to provide the most accurate mode-specific scattering rates because the successful record of simulating mode dependent phonon properties and thermal conductivities (Broido et al. 2005, Garg et al. 2011, Garg & Chen 2013). However, due to the expensive computation costs, only a few papers exist using the normal mode analysis method to examine the mode-specific scattering rates in bulk materials (Garg et al. 2011, Ward & Broido 2010), and the complication associated with nano-phononic crystal simulation. In this chapter, we will use the normal mode analysis based on Green Kubo Molecular Dynamics methods in the well-established open source software, LAMMPS, to calculate the mode-dependent relaxation time.

3.2 Methods to Validate the Assumption

In this section, the phonon dependent lifetime and thermal conductivities of different materials, including bulk Ar, Si, and Ar/heavy Ar QDSL, are calculated using the normal mode analysis (NMA) and Callaway-Holland methods. The key inputs to the Callaway-Holland model (direct summation method) are group velocities, which are obtained from dispersion relations generated with harmonic lattice dynamics calculations (Dove 1993) and relaxation times from established empirical equation models (Gillet et al. 2009, Glassbrenner & Slack 1964, Davis & Hussein 2011). Calculations were performed for various different sized supercells, the periodically repeating building blocks used to generate phononic crystal structure.

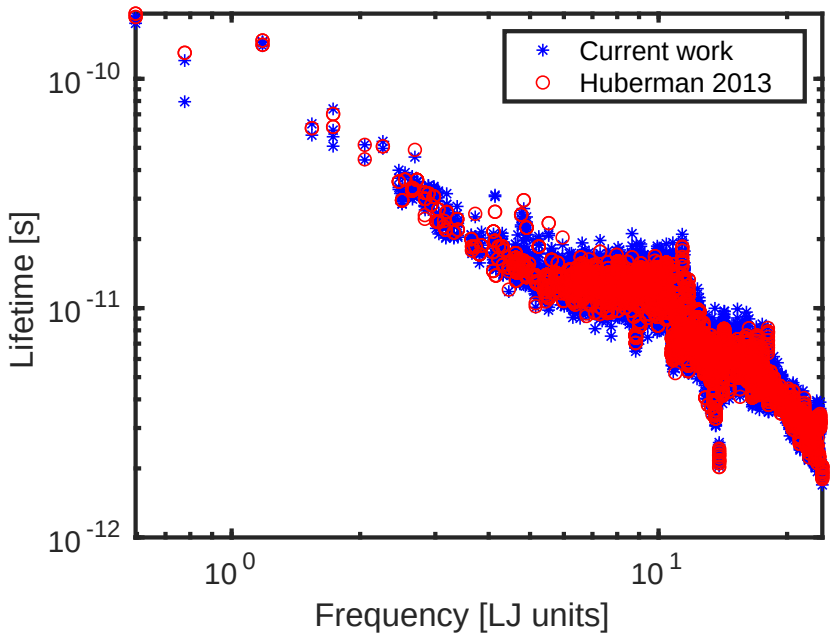

Figure 3.1: Verification of the normal mode analysis method to literature results: Blue stars are result from current work, red circles is result from the reference paper (Huberman 2013). The geometry is Ar heavy Ar superlattices with thickness of 4CCs and length 8x6x6 at T=20K.

3.3 Results

We first verify the NMA method, then calculate thermal conductivity of bulk Ar and Ar/Heavy Ar QDSLs.

3.3.1 Verification of Modeling Methods

Before examining the validity of the assumption of empirical scattering equations, we first verified the normal mode analysis against benchmark data in the literature. The results were compared to the lifetime data computed by Huberman *et al.* (Huberman 2013) for Ar/heavy Ar superlattice as shown in Fig. 3.1. Using the same potentials, geometries, and lattice constants, we obtained very good agreement with Huberman's results (Fig. 3.1).

The empirical equation method in this chapter is same as the direct summation method in Chapter 2. The material is changed from Si and Ge to Ar and heavy

Ar with the Lennard-Jones potential. The τ equation in this chapter is similar to Chapter 2. In general, τ depends on phonon-phonon, phonon-boundary, and phonon-defect scattering (Klemens 1958). In QDSL, it additionally depends on phonon-nanoparticle scattering (Kim & Majumdar 2006, Gillet et al. 2009). In this chapter, the relaxation time for bulk Ar is expressed as $\tau = \left[\tau_U^{-1} + \tau_N^{-1}\right]^{-1}$, where $\tau_U^{-1} + \tau_N^{-1} = (B_1 + B_2)\omega^2 T^3$ represents normal (N) and Umklapp (U) three-phonon scattering. The relaxation time for Ar/Heavy Ar is expressed as $\tau = \left[\tau_U^{-1} + \tau_N^{-1} + \tau_{NP}^{-1} + \tau_I^{-1}\right]^{-1}$, where $\tau_{NP}^{-1} = \eta v\left((\sigma^f)^{-1} + (\sigma^n)^{-1}\right)^{-1}$ represents nanoparticle scattering with $\sigma^f = \pi R^2 \chi^4 h_1(\chi, \Delta M/M, \Delta K/K)$ and $\sigma^n = 2\pi R^2 h_2(\chi, \Delta M/M, \Delta K/K)$. Here η, M, and K are the nanoparticle volumetric density, the mass of the host medium, and force constant of the host medium, and $\chi = qR$ is the size parameter for a scatterer with the characteristic radius $R = a/2$ in this paper. $\tau_I^{-1} = D\omega^4$ represents defect scattering by impurities. For QDSLs, the parameter B in τ_U is taken from the host material's value while the angular frequency is taken from actual dispersion curves. Detailed information about the functions, h_1, and h_2, can be found in Refs. (Kim & Majumdar 2006, Gillet et al. 2009). The values of the parameters used in the relaxation time calculations (Table 3.2) are taken from Refs. (Chen et al. 2004). The heavy Ar atoms have exact same parameters as Ar atoms except the mass, which gives $\Delta M/M = 2$ when the mass ratio is 3.

Table 3.2: Simulation parameters for Ar/Heavy Ar QDSLs with mass ratio of 3

	B1 + B2(sK^{-1})	D(s^3)	$\Delta M/M$	$\Delta K/K$
Ar	$8e-19$	$4.01e-43$	2	0

3.3.2 Bulk Materials

After verifying the Normal Mode Analysis method, the lifetime of bulk Ar with different supercell sizes was calculated using both normal mode analysis and empirical scattering equation methods. Convergence tests for size effect, time effect and q-space resolution effect are conducted first to make sure that results are reasonable, then the thermal conductivity results for bulk Ar is presented.

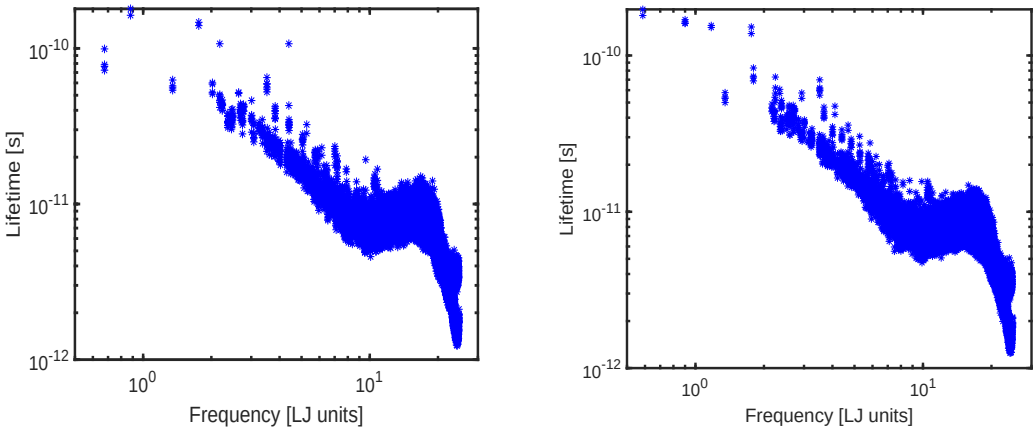

Figure 3.2: Convergence test of bulk Ar for different sizes: (a) bulk Ar 40x10x10 CCs and (b) bulk Ar 60x10x10 CCs.

Convergence Results

Figure 3.2 and Figure 3.3 show that the lifetime results became very stable even when we increase the supercell size and decrease the time interval in each case. In this work, the time interval is how often we store the MD data. Therefore, in the following cases, similar supercell size (8x6x6 CCs) and computation length (2^{20} steps) will be used for the MD calculation for Ar and Ar/HAr QDSLs. To verify the convergence of group velocity calculation and obtain a clear trend, we calculate the cumulative value of the square of the group velocity in the x direction, which is defined as $\sum_0^\omega v_x^2(\omega)$ and plotted in Fig. 3.4. Figure 3.4 with different q-space resolution show that the group velocities achieve stability for q-space intervals d_q below 10^{-5} LJ unit, so the value 10^{-5} LJ unit was used for all calculations.

Lifetime and Thermal Conductivity of Bulk Ar

Figure 3.5 shows one example of the lifetime results from the normal mode analysis for bulk Ar material. To test the size effect of the thermal conductivity from both methods, we calculated the thermal conductivity results for bulk Ar with multiple supercell sizes, which was shown in Figure 3.6. The x-axis shows the supercell size in

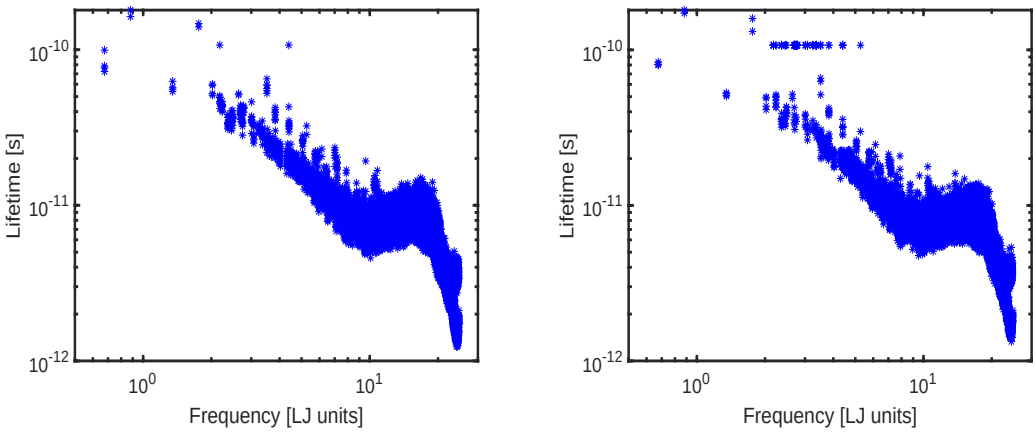

Figure 3.3: Convergence test of bulk Ar for different time intervals in MD: (a) time interval = 32 time steps and (b) time time interval = 16 time steps using bulk Ar 40x10x10 CCs.

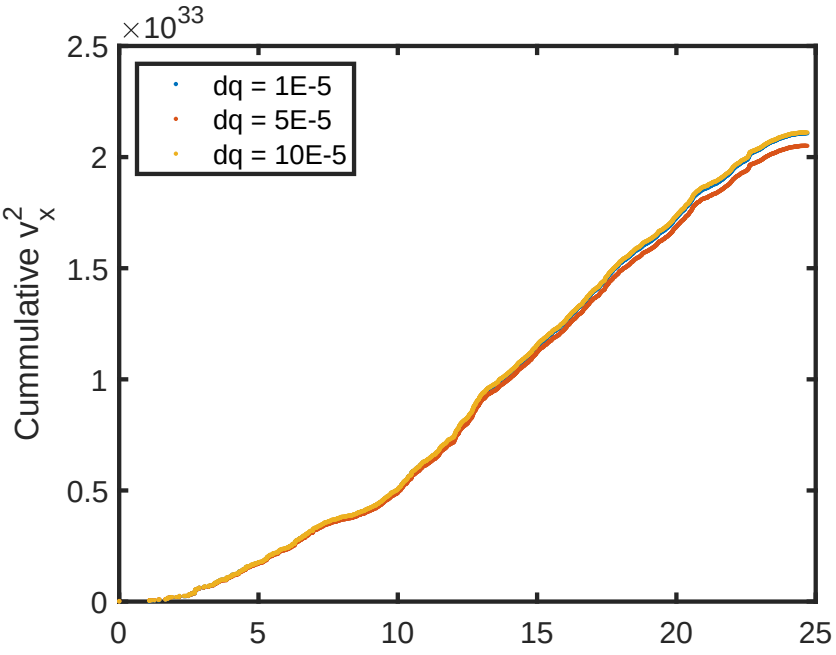

Figure 3.4: Convergence test of velocity in bulk Ar for different q-space resolutions with dq = 10^{-5}, $5x10^{-5}$, and $10x10^{-5}$.

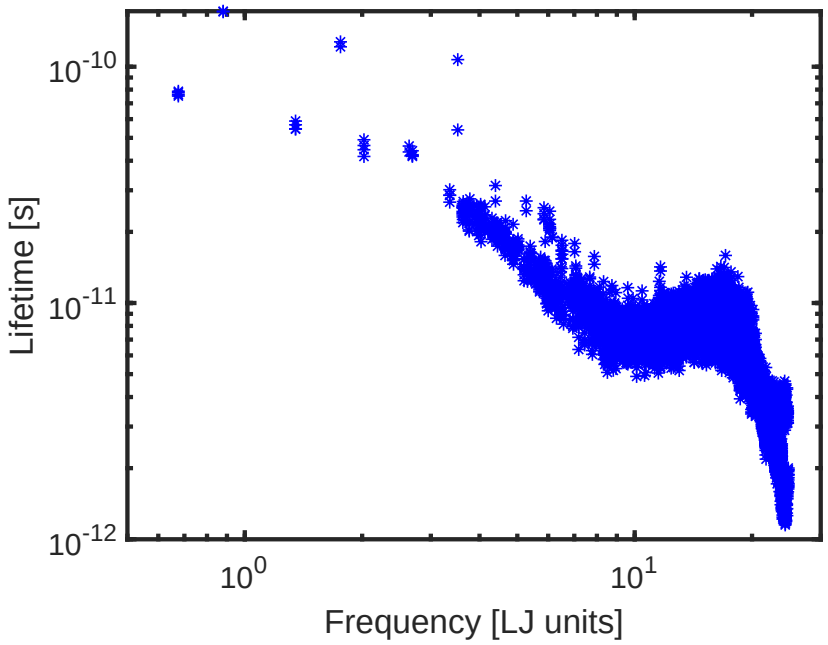

Figure 3.5: Lifetime of bulk Ar using the normal mode analysis method.

CCs for five samples, which are 8x6x6 CCs, 30x8x8 CCs, 40x10x10 CCs, 50x10x10 CCs, 60x10x10 CCs in x,y,z directions. The y-axis represents the thermal conductivity results in [W/mK]. Figure 3.6 shows that both NMA and empirical equations give constant thermal conductivity for all supercell sizes for bulk Ar, as expected. In addition, it also showed that the empirical method results over-estimated the thermal conductivity results compared to the NMA method, which made us doubt the validity of the empirical equation method.

3.3.3 Nano-Phononic Crystals

To examine the validity of the empirical scattering rate assumption further, we compared the results of normal mode analysis and Callaway-Holland models on various QDSL configurations and materials. Ar/heavy Ar QDSLs with supercell side length 3x3x3 CCs of Ar and a single CC of heavy Ar with mass varying from two to five times of Ar in the center, a similar geometry as seen in Fig. 2.1 for Si/Ge QDSL. For both methods and in all QDSL types, the thermal conductivity decreases with the increasing dot masses. This is thought to occur because the mass mismatch could in-

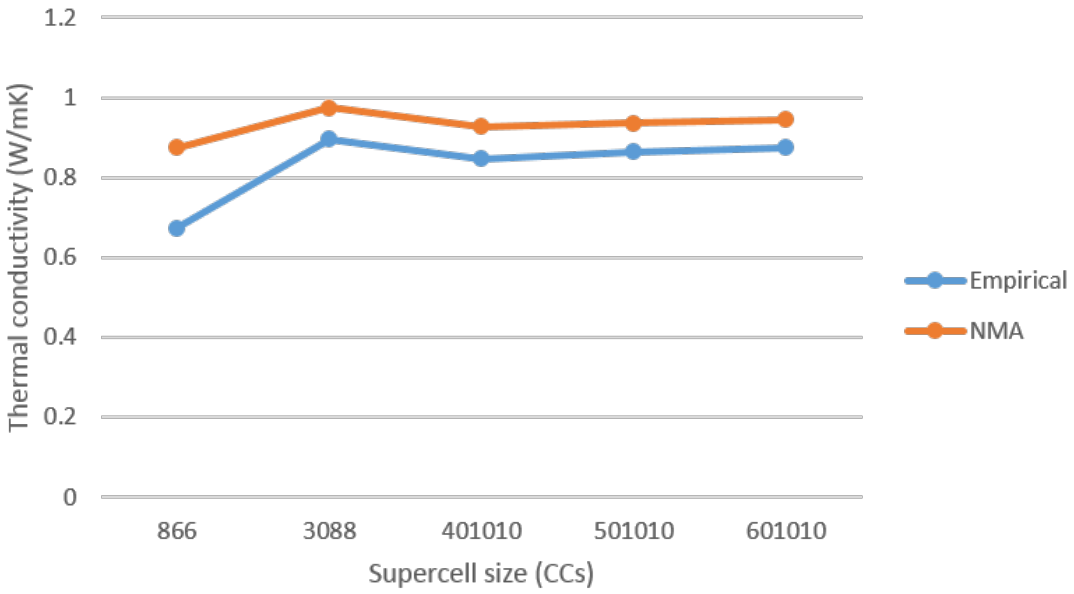

Figure 3.6: Thermal conductivity of bulk Ar with different supercell sizes using the empirical equation and normal mode analysis methods.

crease the scattering events in QDSLs, and the nano particle relaxation time increases relative to the Umklapp and impurity relaxation time as mass mismatch increases. Phonons are reflected at interfaces of different materials, impeding phonon transport and reducing thermal conductivity. In addition, the results of empirical equation method deviated from the results of normal mode analysis, which is also shown as the ratio of k_{EMP}/k_{NMA} in Fig. 3.8. The thermal conductivity ratio goes below 1 for larger mass because the empirical equation method underestimate the results as the mass ratio increases.

The comparison of phonon lifetimes between NMA (which is also called NMD in some literatures) and Empirical for Ar/heavy Ar QDSL with different mass ratio is plotted in Fig. 3.9, where the mass ratio changed from 2 to 5. For both methods and in all QDSL types, the phonon lifetime decreases with increasing frequency. It is also observed that the lifetimes from the NMA method increases at certain high frequency range compared to that of the empirical equation method, which is thought to increase the phonon-nanoparticle relaxation time, which impacts thermal conductivity. In the empirical equation case, the lifetime monotonically decreases as the frequency

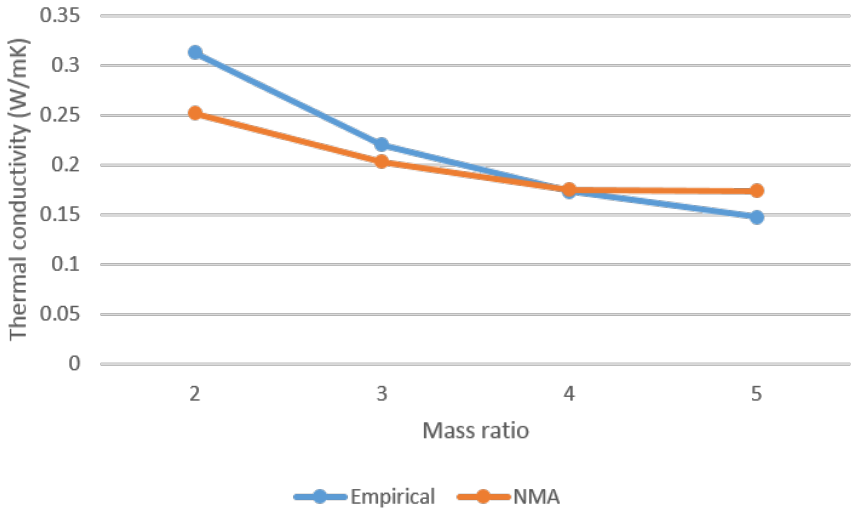

Figure 3.7: Thermal conductivity of Ar/Heavy-Ar QDSL with (different) dot masses using the empirical equation and normal mode analysis methods.

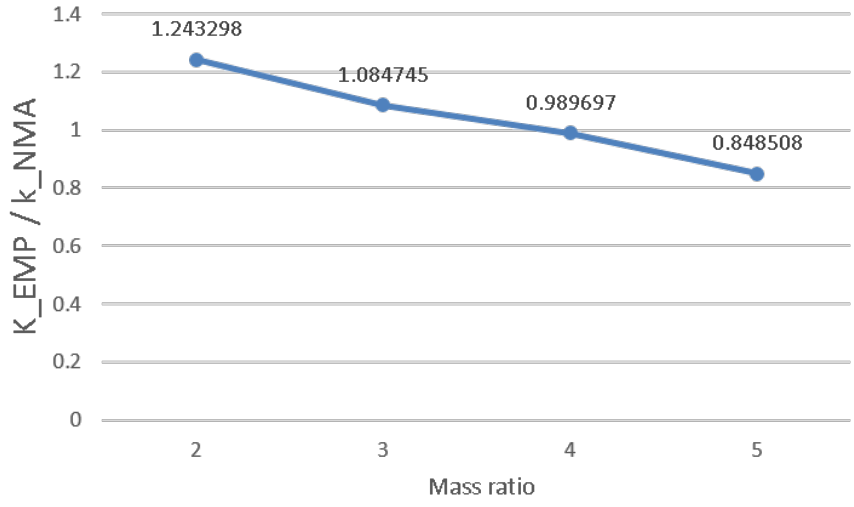

Figure 3.8: The ratio of thermal conductivity results from the empirical equation method and the normal mode analysis method for Ar/H-Ar QDSL with different dot masses.

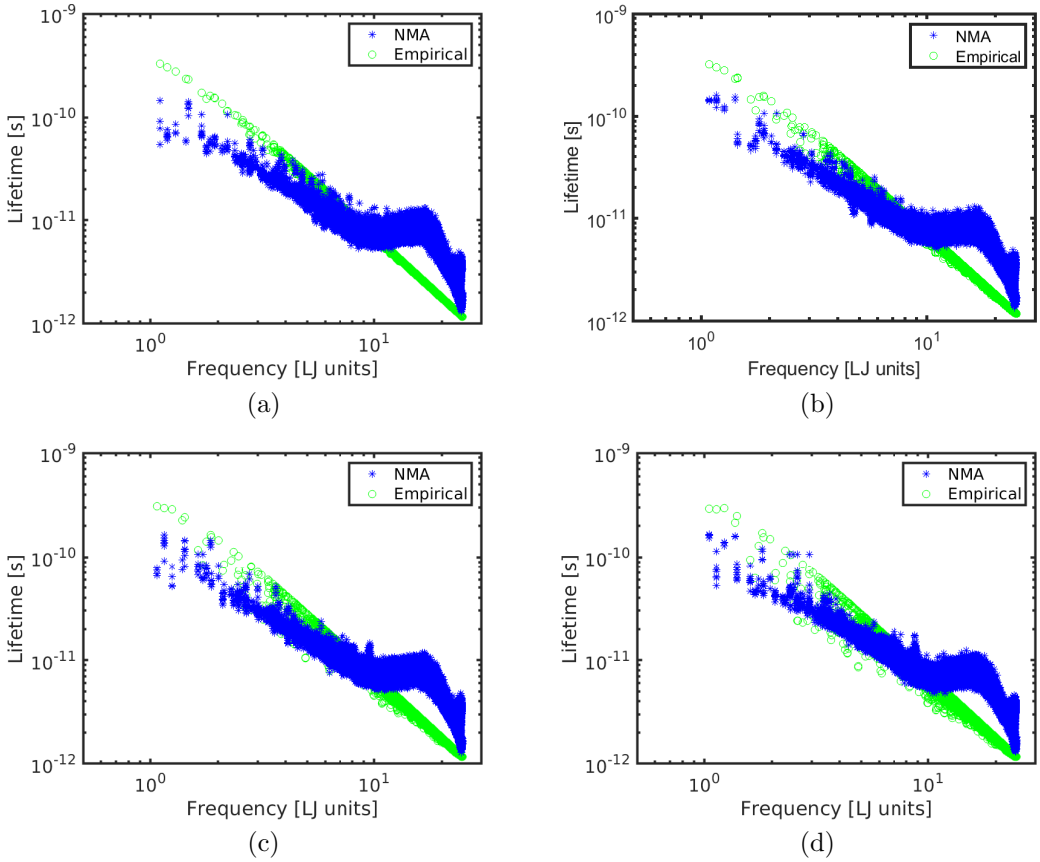

Figure 3.9: Lifetime of Ar/Heavy-Ar QDSL using the empirical equation method (green circles) and normal mode analysis method (blue circles) with different mass ratio: (a) mass ratio = 2, (b) mass ratio = 3, (c) mass ratio = 4, and (d) mass ratio = 5.

increases, which is similar to the trend of bulk Ar.

3.4 Discussion

The difference between the empirical equations and the normal mode analysis methods can be more clearly quantified by calculating the ratio of k_{emp} (Eq. 2) and k_{NMA} (Eq. 1), shown in Fig. 3.8 for Ar/Heavy Ar QDSL, with mass ratio = 2 to 5. For all three cases, the empirical equation thermal conductivity results drift further away from the normal mode analysis results as the mass ratio increases. The change of the ratio from the lightest mass to the heaviest mass is +25% to −20% in all five cases.

All of the previous results show that empirical equation method for thermal conductivity calculation is different from the normal mode analysis method, and that those two methods have a large difference at low mass ratio, goes to zero, then at higher mass ratio increases again. To explain this trend, we would like to revisit the direct summation equation (Eqn 2.7) and analyze the contributions from specific heat, group velocity and relaxation times.

The only difference between the two methods for a specific mass ratio is the relaxation time, however, all the three parameters (specific heat, group velocity and relaxation times) could change the results when we study different mass ratios. Those figures will be presented one by one.

Figure 3.10 showed that the difference of the cumulative value of the mode thermal conductivity between EMP and NMA as a function of frequency, which is defined as $\chi(\omega) = (\sum_0^\omega k_{EMP} - \sum_0^\omega k_{NMA}) / \sum_0^{\omega_{max}} k_{NMA}$, where EMP stands for the empirical equation method. Here we used the cumulative value because it provides a more clear trend than plotting thousands of modes on one figure separately. The cumulative values are frequency dependent, which gives us a direct idea on which part of phonon modes contributes more to the differences. For example, Fig. 3.10 showed that the phonons at low frequency ([3-13] LJ unit) and high frequency ([18-25] LJ unit) behave differently. We can see that the major difference concentrated at certain frequency ranges, and the contributions at those frequency ranges are changing as the mass ratio increases.

Similarly, we defined $\chi_\tau(\omega) = (\sum_0^\omega \tau_{EMP} - \sum_0^\omega \tau_{NMA}) / \sum_0^{\omega_{max}} \tau_{NMA}$ to represent the difference of the cumulative value of the mode lifetime between the empirical and NMA methods. Figure 3.11 illustrates the difference of χ_τ for different mass ratios quantitatively and we found that χ_τ doesn't change significantly with increasing mass ratio, which is different from the function χ in Fig. 3.10. This finding seems counterintuitive at first since the only difference between the empirical equation and normal mode analysis for a specific mass ratio is τ. However, other two parameters C_p, v_x could change with increasing mass ratio, resulting in the difference between the two methods.

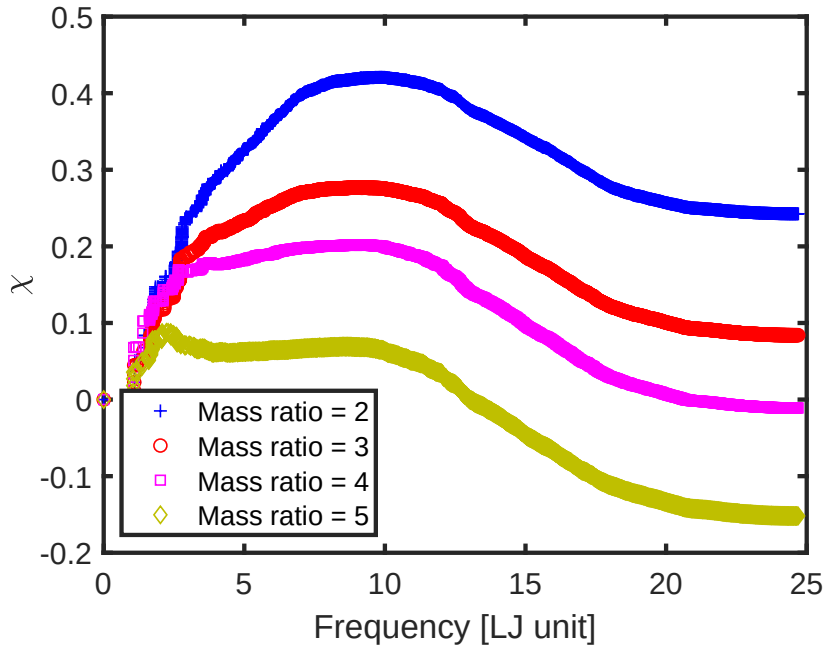

Figure 3.10: The difference of cumulative mode thermal conductivity between two methods, χ, as function of frequency for different mass ratios.

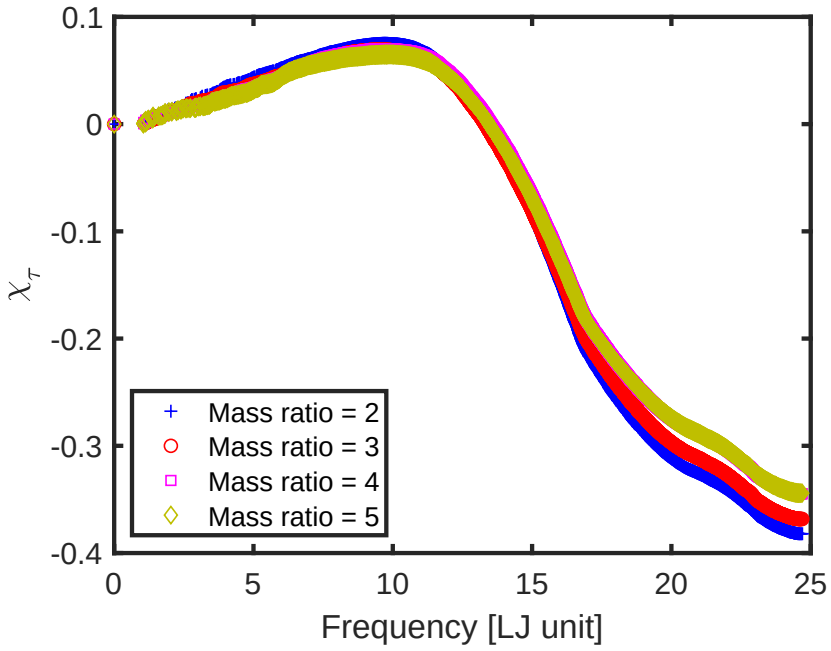

Figure 3.11: The difference of cumulative mode lifetime between two methods, χ_τ as a function of frequency for different mass ratios.

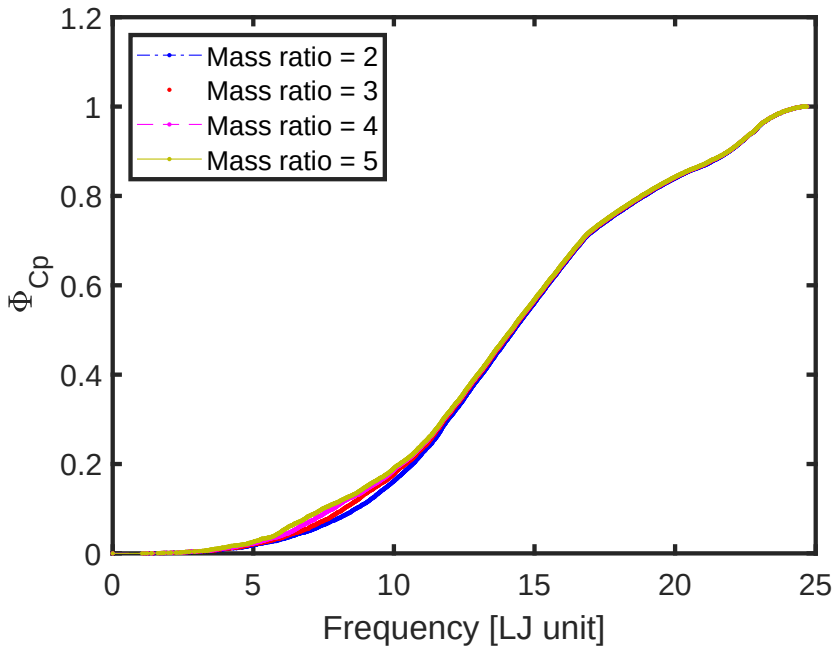

Figure 3.12: The normalized cumulative values of mode Cp, Φ_{C_p}, as a function of frequency for different mass ratios.

Next, we break down the Equation 2.7 into C_p, v^2 and τ to study which parameter is the key driver for the difference between the empirical equation and normal mode analysis methods. To obtain a clear trend, we defined a general normalized cumulative function for any parameter f versus frequency, $\Phi_f(\omega) = \sum_0^\omega f(\omega) / \sum_0^{\omega_{max}} f(\omega)$. Therefore $\Phi_{C_p * v_x^2}$, Φ_{C_p}, $\Phi_{v_x^2}$ represent the normalized cumulative functions of three different parameters, which could clearly show us the fundamental difference.

The normalized cumulative functions of C_p and v^2 are plotted in Fig. 3.12 and Fig. 3.13. It's obvious that C_p has very little contribution to the difference while v^2 contributes most to the change. Since we have tested the accuracy of the group velocity calculation with different q-space resolutions (Fig. 3.4), the results are reliable. To directly compare those parameters with different mass ratios, we plotted the summation value of C_p, v^2, τ versus mass ratio for both NMA and empirical methods, as shown in Fig. 3.14, Fig. 3.15, and Fig. 3.16. Those figures clearly showed that there is no significant dependence on mass ratio for parameters C_p and τ, while we see the dependence on mass ratio for v_x^2.

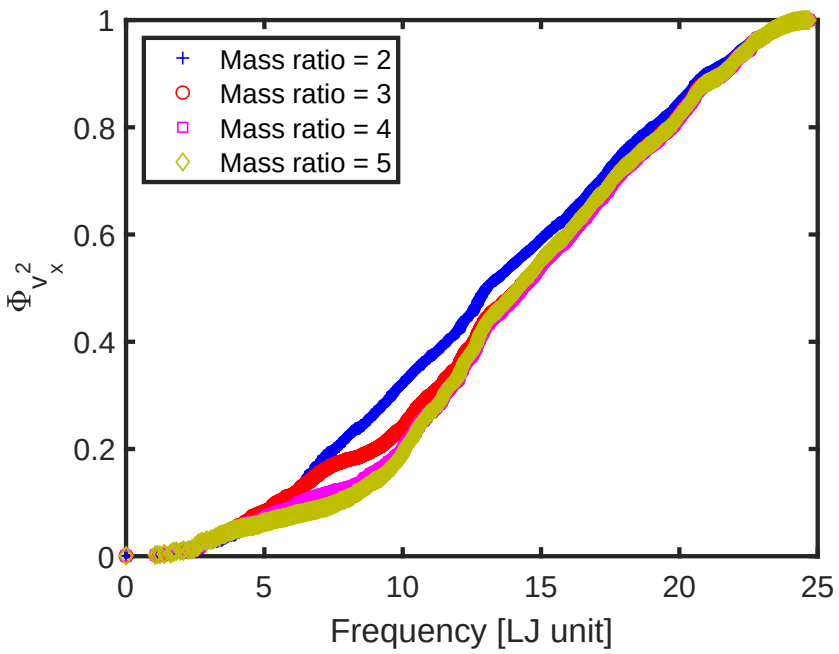

Figure 3.13: The normalized cumulative values of mode v_x^2, $\Phi_{v_x^2}$, as a function of frequency for different mass ratios.

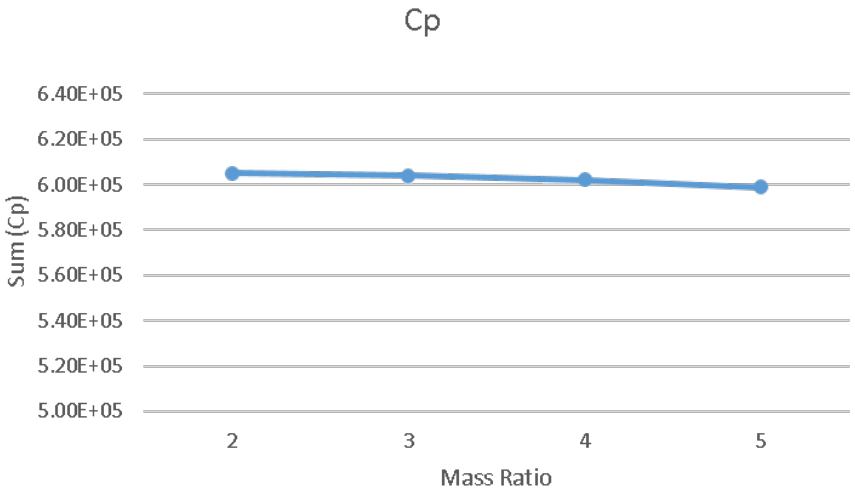

Figure 3.14: The summation of Cp for different mass ratio.

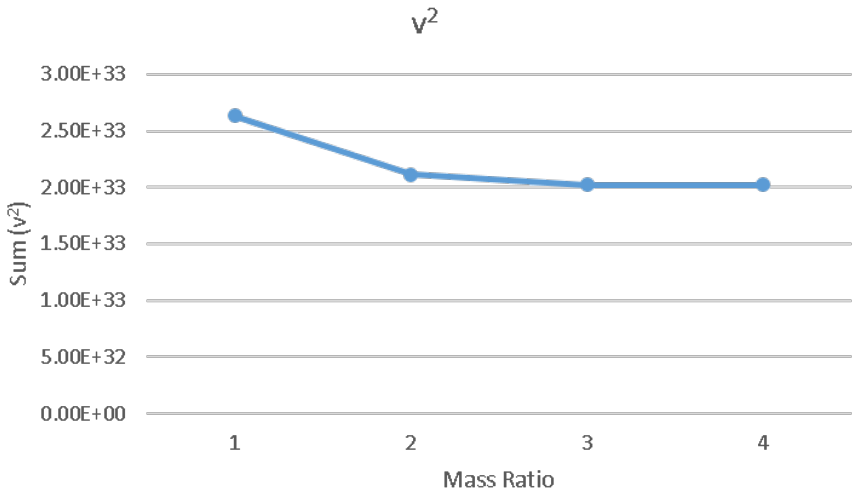

Figure 3.15: The summation of v^2 for different mass ratio.

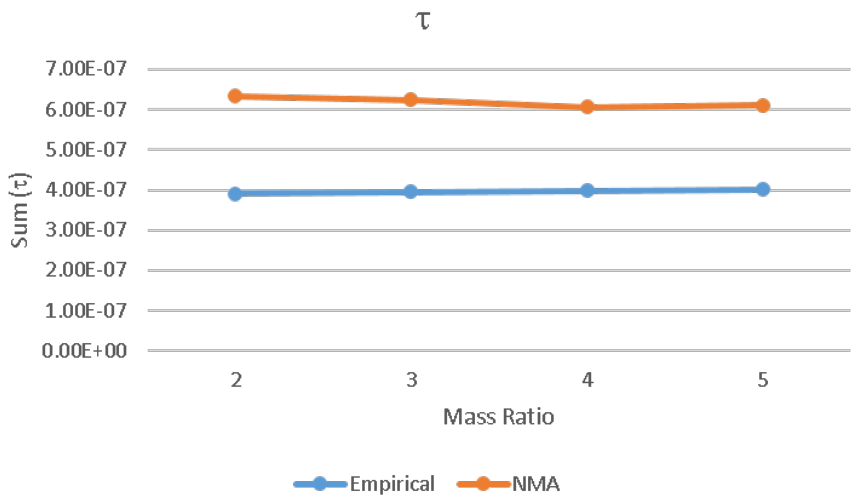

Figure 3.16: The summation of τ from empirical equation and NMA methods for different mass ratio.

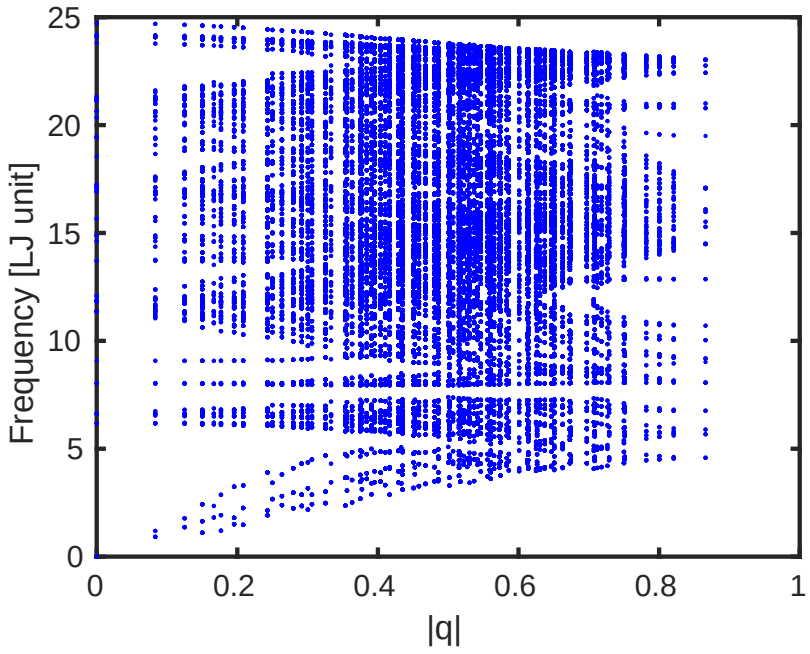

Figure 3.17: The dispersion curve of Ar/Heavy Ar QD (2x2x2 CCs and mass ratio = 5) with a mini-bandgap at [7.1 - 8.1] frequency range.

The behavior could be understood in the following way. As the mass ratio increases, the dispersion curves of the quantum dot are depressed and the velocity have huge reduction, which was clearly illustrated by the mini-bandgap on the dispersion curve in Fig. 3.17 for Ar/heavy Ar QDSL with supercell size of 2x2x2 CCs and mass ratio of 5. This idea of group velocity reduction was also discussed in literature (Yang & Chen 2003) for GaAs/AlAs superlattices. Overall, the only difference between the empirical equation and normal mode analysis methods at a specific mass ratio is τ, which changes little when the mass ratio increases. However, the group velocity reduction caused by the increasing mass ratio significantly changes the differences between those two methods.

3.5 Conclusions

In summary, we found three major conclusions from the comparison of thermal conductivities calculated from the normal mode analysis and empirical equation methods. First, the empirical equation method cannot replicate the normal mode analysis re-

sults, especially in the high frequency range. Second, the thermal conductivity results from the empirical equation deviates from those of the normal mode analysis when the mass of the quantum dot increases. Finally, the group velocity reduction caused by the increasing mass ratio significantly changes the differences between those two methods while the difference of lifetime between those two methods are relatively stable.

Chapter 4

Examination of the Effective Material Assumption for Nano-Phononic Crystals

This chapter analyzes the validity of the third assumption in the Callaway-Holland model for nano-phononic crystals: the effective material assumption. We are going to first look at the literatures which covers the effective material assumptions. We then introduce the Green Kubo Modal Analysis (GKMA) method which will be used to evaluate the effective material assumption by comparing it to the normal mode analysis method. The GKMA method directly determines mode-dependent thermal conductivities from modal heat flux instead of calculating intermediate parameters such as C_p, v_x, τ. The results from the GKMA and NMA methods will be presented and discussed. Finally, the conclusion about the validity of the effective material assumption will be presented.

4.1 Literature Reviews on Previous Work

4.1.1 Optical Meta-Material Versus Photonic Crystals

As discussed in section 1.3.2, the fundamental problem with equations (1.15), (1.11) and (1.12) as applied to nano-phononic materials is that they treat the material as a single bulk material with effective properties. A more accurate BTE-based method would be to directly simulate phonon transport in nano phononic materials, by representing each region with different material properties, and interfaces, and computing the heat flux from the temperature gradient.

However, as the supercell size of nano-phononic crystal increases, phonons with wavelengths shorter than the supercell size will be incorrectly calculated, such as the frequencies and group velocities of those phonon modes (Ma & Lukes 2018). This idea that the periodic composites with different geometry parameters show different properties is not a new concept in optics, which can been seen in the transitions from meta-material to photonic crystals (Rybin et al. 2015). In optical meta-materials, the effective material assumption is valid because the wavelength of light is much longer than the periodicity of the material. However, the effective material assumption cannot capture the actual physics in the photonic crystals when the wavelength is of the order of the periodicity. Concerns on the incorrect calculation for shorter wavelength phonons raises questions on the validity of the effective material assumption in nano-phononic crystals. The development of Green Kubo modal analysis (GKMA) (Lv & Henry 2016), based on the heat current function in the Green Kubo Molecular Dynamics method, gives us the advantage to evaluate the validity of the effective material assumption of the Callaway-Holland model in nano-phononic crystals.

4.1.2 Virtual Crystal Assumption

The effective material assumption is similar to the virtual crystal assumption, in which the disordered materials and the mixture of two or more pure crystals have phonon properties that are compositionally weighted averages of the phonon properties of

the constituent base crystals. The virtual crystal approximation has been used in the thermal properties calculation for alloys (Larkin & McGaughey 2013, Huberman et al. 2013) and disordered materials (Larkin 2013). Henry and et al. (Lv & Henry 2016, Seyf et al. 2017) have shown that the virtual crystal approximation in disordered materials is inaccurate by comparing the GKMA and virtual crystal assumption thermal conductivity results for $In_{0.53}Ga_{0.47}$ thin film. In this work, we want to compare the difference between those two methods for nano-phononic crystals.

4.1.3 Introduction of GKMA Method

The GKMA approach is a totally different thermal conductivity approach. It is not based on BTE so it does not make any assumption about effective C_p, v, τ. It is based on the heat current autocorrelation. The Green Kubo Modal Analysis (GKMA) method (Lv & Henry 2016, Seyf et al. 2017) is explained as follows.

First, we need to define the normal mode:

$$X(\vec{q},\lambda) = \frac{1}{N^{1/2}} \sum_{jl} m_j^{1/2} exp(-i\vec{q}\cdot\vec{r}(jl) e^*(j,\vec{q},\lambda)\cdot\vec{u}(jl,t)). \tag{4.1}$$

Then the velocity of the normal mode can be calculated by

$$\dot{X}(\vec{q},\lambda) = \frac{1}{N^{1/2}} \sum_{jl} m_j^{1/2} exp(-i\vec{q}\cdot\vec{r}(jl) e^*(j,\vec{q},\lambda)\cdot\dot{\vec{u}}(jl,t)). \tag{4.2}$$

The velocity of atoms can be calculated by

$$\dot{\vec{u}}(jl,t) = \frac{1}{(Nm_j)^{1/2}} \sum_{q,\gamma} exp(i\vec{q}\cdot\vec{r}(l)) e(j,\vec{q},\gamma)\cdot\dot{X}(\vec{q},\lambda)). \tag{4.3}$$

The heat flux Q can be calculated in the following equation:

$$Q(q,\lambda) = \frac{1}{V} \sum_i (E_i \dot{\vec{u}}_i(q,\lambda) + \sum_j (-\nabla_{r_i}\Phi_j \dot{\vec{u}}_i(q,\lambda)\cdot\vec{r}_{ij}), \tag{4.4}$$

where $\dot{\vec{u}}_i(q,\lambda) = \frac{1}{(Nm_j)^{1/2}} exp(i\vec{q}\cdot\vec{r}(l)) e(j,\vec{q},\lambda)\cdot\dot{X}(\vec{q},\lambda)$ is the basic component in equation 4.3, λ is phonon mode index, and V is the volume of supercell, E_i is the sum of

potential and kinetic energy of atom i, Φ_j is the potential energy of atom j, and r_{ij} is the distance between atom i and j.

The thermal conductivity over individual mode contribution is expressed as:

$$k(q,\lambda) = \frac{V}{k_B T^2} \int_0^\infty \langle Q(q,\gamma,t) \cdot Q(0) \rangle, \tag{4.5}$$

in which k_B is Boltzmann constant and T is temperature.

4.2 Method to Validate the Assumption

The main idea of validating the effective material assumption is to conduct a systematic comparison for two sets of calculations. The first set is the Green Kubo Modal Analysis (GKMA) method where the modal thermal conductivity for bulk materials and nano-phononic crystals are calculated directly from Green Kubo formula for modal heat fluxes. The second set is the normal mode analysis (NMA method) (Turney 2009) where the phonon properties (such as lifetimes) are extracted from the GKMD and spectral energy density (1.12) to calculate the modal thermal conductivity. By comparing the modal results from these two methods, we expect to have a basic idea on how accurate the effective material assumption is in the thermal conductivity calculation for nano-phononic crystals. The modal thermal conductivities of bulk Ar and Ar/heavy Ar QDSLs will be discussed in this section.

4.3 Results

4.3.1 Verification of GKMA method

Before examining the validity of the effective material assumption, we first verified the GKMA method against the literature results or traditional Green Kubo molecular dynamics. The geometry is bulk Ar with 6x6x6 conventional cells. The thermal conductivity of bulk Ar using GKMA at $T = 20K$ is plotted in Fig. 4.1, with the heat current autocorrelation function. The thermal conductivity result from GKMA

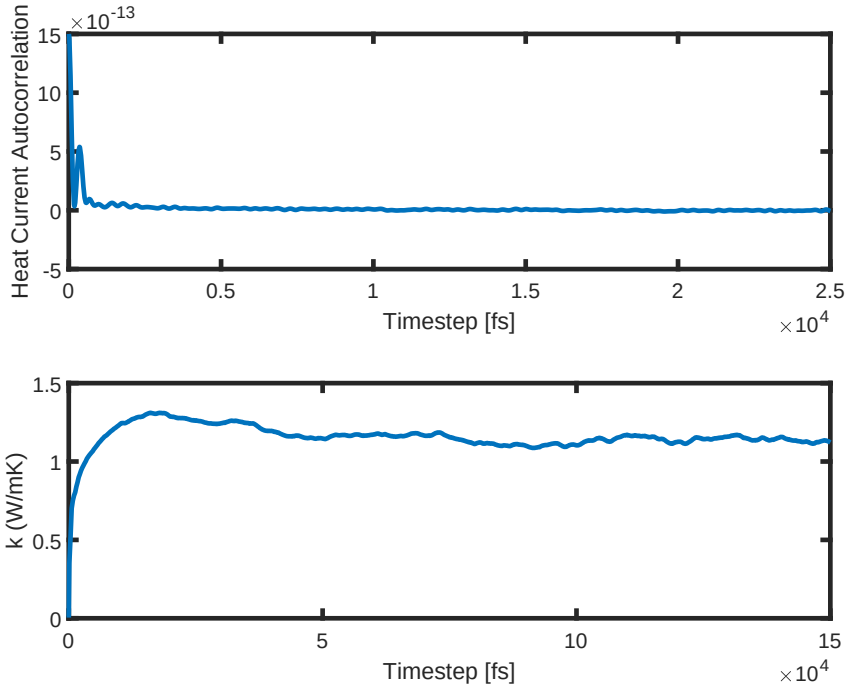

Figure 4.1: Heat current autocorrelation function (top) and thermal conductivity (bottom) of GKMA method for bulk Ar with 6x6x6 CCs at T = 20 K.

method averaged from $5e4 - 15e4$ [fs] in Fig. 4.1 is 1.14 W/mK, which matches well with literature papers (McGaughey & Kaviany 2004). Figure 4.2 showed that the thermal conductivities for bulk Ar at $T = 50K$ from five cases with different initial velocities. The average value of those five cases, the bold magenta line averaged from $5e4 - 15e4$ [fs], is 0.305 W/mK, which agrees with the results from literature paper (McGaughey & Kaviany 2004) too. Overall, we obtained good agreement between GKMA results and the benchmark results.

4.3.2 Nano-Phononic Crystals

Limited cases for nano-phononic crystal thermal conductivity calculation using Green Kubo Modal Analysis (GKMA) method have been conducted because the modal thermal conductivity calculation is computationally very expensive. The basic cell is same as the Ar/heavy Ar QDSLs we used in the last chapter: 3x3x3 conventional cells (CCs) of Ar with 1x1x1 CCs of heavy Ar with mass of 3 times of normal Ar. The

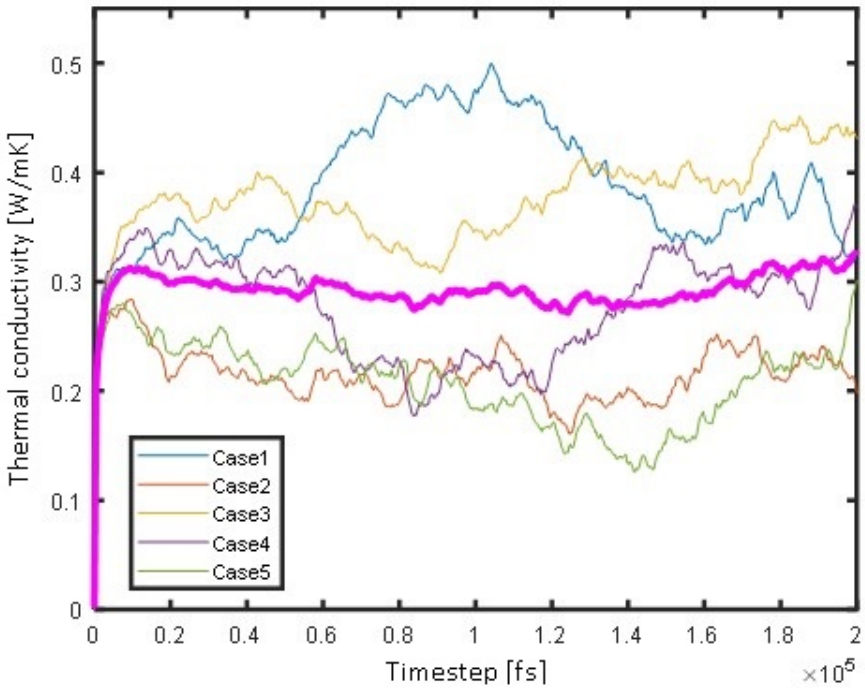

Figure 4.2: Thermal conductivity of GKMA method for bulk Ar at T=50K using a 4x4x4 conventional cell. Bold magenta line is the average thermal conductivity of five initializations.

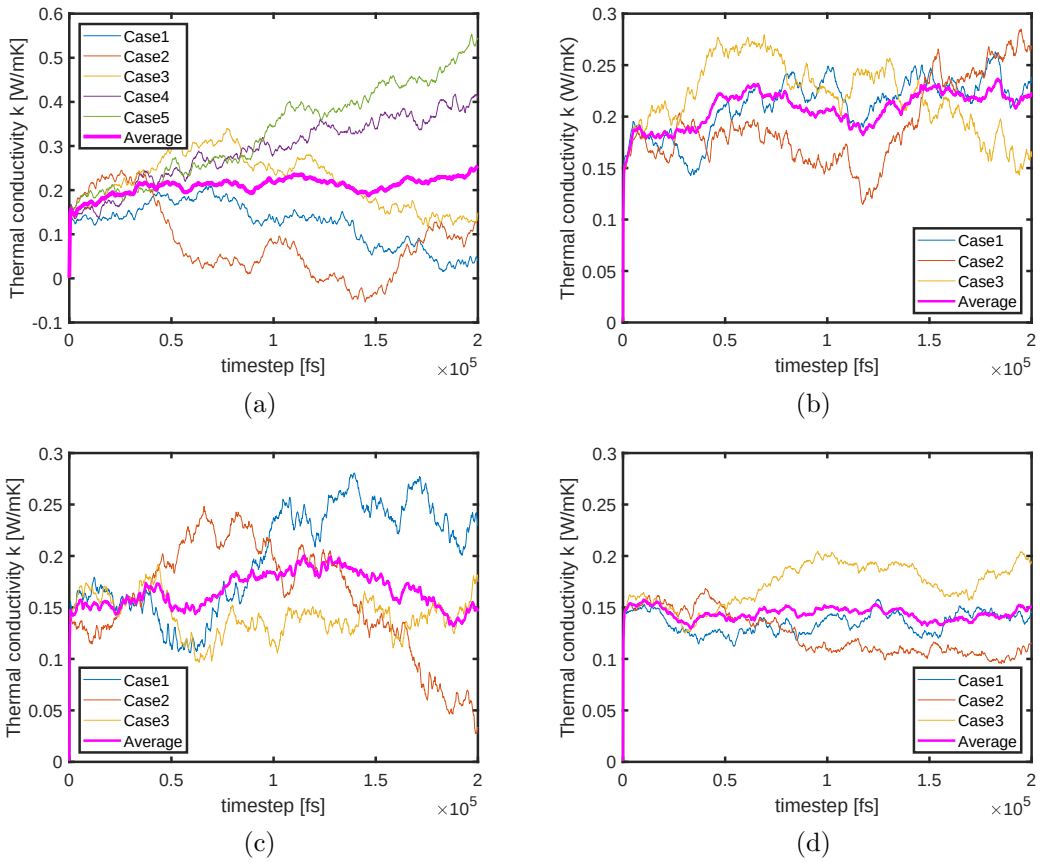

Figure 4.3: Thermal conductivity of GKMA method for Ar/heavy Ar with 3x3x3-2x2x2 CCs at T = (a) 20 K, (b) 30 K, (c) 40 K, and (d) 50 K.

basic cell is then repeated several times in x, y, z directions (two times in this work, 3x3x3-2x2x2) to stabilize the calculation data. The thermal conductivity result for the Ar/heavy Ar QDSL (3x3x3-2x2x2) with full size of 6x6x6 CCs at $T = 20, 30, 40, 50K$ were plotted in Fig. 4.3.

The thermal conductivity result of the Ar/heavy Ar QD in Fig. 4.3 from GKMA method is $0.21W/mK$ from GKMA method at $T = 20K$, and $0.17W/mK$ at $T = 50K$. In comparison, the thermal conductivity results for the same geometries using the GKMA method and normal mode analysis (NMA) methods are listed in the Table 4.1. Even though the thermal conductivities from both results are close enough at $T = 20K$, they have a sizable difference at high temperatures $T = 50K$. The reason may be that normal mode analysis cannot correctly capture the thermal conductivity

contribution of the short wavelength phonon modes excited at high temperature.

Table 4.1: Thermal conductivity from GKMA and NMA methods $[W/mK]$

T	$20(K)$	$30(K)$	$40(K)$	$50(K)$
GKMA	0.220	0.18	0.162	0.150
NMA	0.213	0.164	0.137	0.114

4.4 Conclusion

The Green Kubo Modal Analysis (GKMA) method is verified in this chapter, and applied in bulk Ar, and Ar/heavy Ar QDSLs. A simple comparison between GKMA and NMA for Ar/heavy Ar QD (3x3x3) at different temperatures has been conducted. Those results agreed well at low temperature $20K$, however, it deviated at high temperature. This difference could imply that the normal mode analysis may not correctly capture the phonon behaviors at high temperature.

Chapter 5

Conclusions

5.1 Summary and Contributions

The following is a summary of the most important contributions made by this dissertation.

Nano-phononic crystals are periodic structures characterized by band gaps in the frequency spectrum that present surprising and transformable properties. Correctly simulating thermal propagation of these materials is essential for optimizing and tuning their properties. The different assumptions involved in the Callaway-Holland model makes it challenging to accurately predict thermal conductivities of nano-phononic crystals.

First, this dissertation investigated the isotropic thermal conductivity assumption by benchmarking it with direct summation method for thermal conductivities in bulk Si, Si/Ge QDSLs, and Ge/Si QDSLs. The direct summation method yields the same bulk Si thermal conductivity value with different supercell sizes, which is physically meaningful and comparable with results from other works. The difference between the direct summation and isotropic methods depends substantially on the supercell size for both bulk Si and Si/Ge quantum dot superlattices. The thermal conductivity contribution from phonons neglected in the isotropic assumption calculations increases as supercell size increases, which can be explained by the increased relaxation time of neglected phonons. While significantly smaller than the effect of

Brillouin zone shape, the effect of crystal anisotropy has a non-negligible contribution to the thermal conductivity dependence on supercell size.

Second, this dissertation provided several conclusions when examining the empirical relaxation time assumption. The empirical potentials cannot replicate the normal mode analysis results, which was following the $\tau \sim \omega^{-2}$ rule at the low frequency and a peak in the high frequency range. In addition, the thermal conductivity results from the empirical potential deviates from those of the normal mode analysis when the mass of the quantum dot increases. The fundamental reasons behind the deviation is because of the group velocity, which produces the difference between the contribution from the two methods as the mass of quantum dot changes.

Third, The Green Kubo Modal Analysis (GKMA) method is verified in this dissertation, and applied in bulk Ar, and Ar/heavy Ar QDSLs. A simple comparison between GKMA and NMA for Ar/heavy Ar QD at different temperatures have been conducted. Those results agreed well at low temperature $20K$, however, it deviated at high temperature. This difference could imply that the normal mode analysis may not correctly capture the phonon behaviors at high temperature, and Green Kubo Modal Analysis method is recommended when considering effective material assumption.

Overall, this work quantitatively evaluated the three major assumptions associated with the Callaway-Holland model for thermal conductivity calculations for nano-phononic crystals, which provides directions for future researchers on how to simulate the thermal conductivity of nano-phononic crystals correctly.

5.2 Challenges

There are a lot of challenges in simulating the thermal conductivity of nano-phononic crystals. The biggest one is that normal mode analysis and Green Kubo Modal Analysis methods are computationally expensive. The normal mode analysis has a heavy demand on storage, which may easily reach to 500 GB for a system with supercell size of 10nm and 1000 wave-vectors in the q-space. The Green Kubo Modal Analysis method could take 1 week for a system of 5nm when considering all the phonon

modes and wave-vectors at the same time. The computational expensiveness makes the simulation really difficult. The future researchers should be aware of those challenges. To provide benchmarks, the isotropic thermal conductivity assumption based Callaway Holland model only takes several minutes, while the direction summation method may takes 2-3 days for same geometries. The time for the normal mode analysis method varies from several hours to several days based on the simulation cell and q-space resolution, and it easily takes more than 5 days for the Green Kubo Modal Analysis to obtain reasonable results.

5.3 Future Directions

Nano-phononic crystals provide great opportunities for realizing and engineering interesting thermal and phononic behavior. One important extension of this work could include analyzing the phonon modal contribution in the Green Kubo Modal Analysis method. Different phonon modes may behave and contribute differently to the thermal conductivity in nano-phononic crystals. The modal phonon behavior is critical to understand the effective material assumption in nano-phononic crystals.

Another interesting future direction is to use the first principles based calculations for more accurate thermal conductivity simulations. First principle method is supposed to provide the most accurate thermal conductivity results for nano-materials, but also demands extensive computational resources. It may also be interesting in this field to develop the accurate interatomic forces form first principles and quantum chemistry, which could provide a framework for interactions between different atoms in nano-phononic crystals.

Appendix A

Group Velocity

Accurate calculations of group velocity are important for thermal conductivity calculations in this paper. For future reference by the research community, we have plotted two examples of [100] direction group velocities computed in this work in Fig. A.1. The branch dependent phonon group velocities for bulk Si and for the Si3Ge1 QDSL in Fig. A.1 show that our group velocity method can clearly distinguish phonons from different branches.

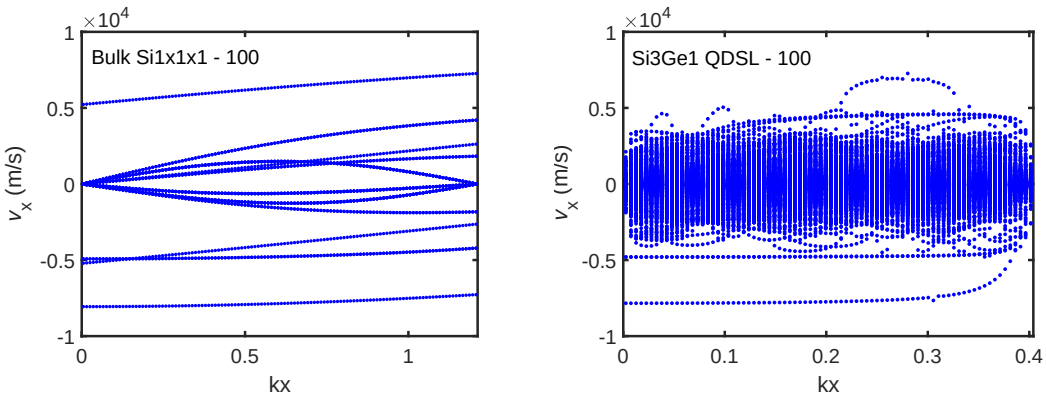

(a) (b)

Figure A.1: Phonon group velocities from different branches along the [100] direction in (a) bulk Si with 1x1x1 CCs and (b) Si3Ge1 QDSL.

Bibliography

Alaie, S., Goettler, D. F., Su, M., Leseman, Z. C., Reinke, C. M. & El-Kady, I. (2015), 'Thermal transport in phononic crystals and the observation of coherent phonon scattering at room temperature', *Nature communications* **6**, 7228.

Anufriev, R. & Nomura, M. (2017), 'Heat conduction engineering in pillar-based phononic crystals', *Physical Review B* **95**(15), 155432.

Berman, R., Foster, E. & Ziman, J. (1955), 'Thermal conduction in artificial sapphire crystals at low temperatures i. nearly perfect crystals', *Proc. R. Soc. Lond. A* **231**(1184), 130–144.

Berman, R. & Ziman, J. (1953), 'The thermal conductivity of diamond at low temperatures', *Proc. R. Soc. Lond. A* **220**(1141), 171–183.

Broido, D., Malorny, M., Birner, G., Mingo, N. & Stewart, D. (2007), 'Intrinsic lattice thermal conductivity of semiconductors from first principles', *Applied Physics Letters* **91**(23), 231922.

Broido, D., Ward, A. & Mingo, N. (2005), 'Lattice thermal conductivity of silicon from empirical interatomic potentials', *Physical Review B* **72**(1), 014308.

Callaway, J. (1959), 'Model for lattice thermal conductivity at low temperatures', *Physical Review* **113**(4), 1046.

Cargnello, M., Johnston-Peck, A. C., Diroll, B. T., Wong, E., Datta, B., Damodhar, D., Doan-Nguyen, V. V., Herzing, A. A., Kagan, C. R. & Murray, C. B. (2015), 'Substitutional doping in nanocrystal superlattices', *Nature* **524**(7566), 450.

Casimir, H. (1938), 'Note on the conduction of heat in crystals', *Physica* **5**(6), 495–500.

Chen, G. (2005), *Nanoscale energy transport and conversion*, Oxford University Press, New York.

Chen, Y., Lukes, J. R., Li, D., Yang, J. & Wu, Y. (2004), 'Thermal expansion and impurity effects on lattice thermal conductivity of solid argon', *The Journal of chemical physics* **120**(8), 3841–3846.

Chernatynskiy, A. & Phillpot, S. R. (2015*a*), 'Anharmonic properties in m g 2 x (x= c, si, ge, sn, pb) from first-principles calculations', *Physical Review B* **92**(6), 064303.

Chernatynskiy, A. & Phillpot, S. R. (2015*b*), 'Phonon transport simulator (phonts)', *Computer Physics Communications* **192**, 196–204.

Davis, B. L. & Hussein, M. I. (2011), 'Thermal characterization of nanoscale phononic crystals using supercell lattice dynamics', *AIP Advances* **1**(4), 041701.

Davis, B. L. & Hussein, M. I. (2014), 'Nanophononic metamaterial: Thermal conductivity reduction by local resonance', *Physical Review Letters* **112**(5), 055505.

Debernardi, A., Baroni, S. & Molinari, E. (1995), 'Anharmonic phonon lifetimes in semiconductors from density-functional perturbation theory', *Physical review letters* **75**(9), 1819.

Dechaumphai, E. & Chen, R. (2012), 'Thermal transport in phononic crystals: the role of zone folding effect', *Journal of Applied Physics* **111**(7), 073508.

Deinzer, G., Birner, G. & Strauch, D. (2003), 'Ab initio calculation of the linewidth of various phonon modes in germanium and silicon', *Physical Review B* **67**(14), 144304.

Dove, M. T. (1993), *Introduction to lattice dynamics*, Vol. 4, Cambridge university press.

El-Kady, I., Olsson III, R. H., Hopkins, P. E., Leseman, Z. C., Goettler, D. F., Kim, B., Reinke, C. M. & Su, M. F. (2012), 'Phonon manipulation with phononic crystals', *Sandia National Labs, Albuquerque, NM, Report No. SAND2012-0127* .

Esfarjani, K., Chen, G. & Stokes, H. T. (2011), 'Heat transport in silicon from first-principles calculations', *Physical Review B* **84**(8), 085204.

Esfarjani, K. & Stokes, H. T. (2008), 'Method to extract anharmonic force constants from first principles calculations', *Physical Review B* **77**(14), 144112.

Evans, D. J. (1982), 'Homogeneous nemd algorithm for thermal conductivityapplication of non-canonical linear response theory', *Physics Letters A* **91**(9), 457–460.

Feng, T. & Ruan, X. (2014), 'Prediction of spectral phonon mean free path and thermal conductivity with applications to thermoelectrics and thermal management: a review', *Journal of Nanomaterials* **2014**.

Garg, J., Bonini, N. & Marzari, N. (2011), 'High thermal conductivity in short-period superlattices', *Nano letters* **11**(12), 5135–5141.

Garg, J. & Chen, G. (2013), 'Minimum thermal conductivity in superlattices: A first-principles formalism', *Physical Review B* **87**(14), 140302.

Gillet, J.-N., Chalopin, Y. & Volz, S. (2009), 'Atomic-scale three-dimensional phononic crystals with a very low thermal conductivity to design crystalline thermoelectric devices', *Journal of Heat Transfer* **131**(4), 043206.

Glassbrenner, C. & Slack, G. A. (1964), 'Thermal conductivity of silicon and germanium from 3 k to the melting point', *Physical Review* **134**(4A), A1058.

Graczykowski, B., Sledzinska, M., Alzina, F., Gomis-Bresco, J., Reparaz, J., Wagner, M. & Torres, C. S. (2015), 'Phonon dispersion in hypersonic two-dimensional phononic crystal membranes', *Physical Review B* **91**(7), 075414.

Henry, A. S. & Chen, G. (2008), 'Spectral phonon transport properties of silicon based on molecular dynamics simulations and lattice dynamics', *Journal of Computational and Theoretical Nanoscience* **5**(2), 141–152.

Holland, M. (1963), 'Analysis of lattice thermal conductivity', *Physical Review* **132**(6), 2461.

Honarvar, H., Yang, L. & Hussein, M. I. (2016), 'Thermal transport size effects in silicon membranes featuring nanopillars as local resonators', *Applied Physics Letters* **108**(26), 263101.

Hopkins, P. E., Rakich, P. T., Olsson, R. H., El-Kady, I. F. & Phinney, L. M. (2009), 'Origin of reduction in phonon thermal conductivity of microporous solids', *Applied Physics Letters* **95**(16), 161902.

Hopkins, P. E., Reinke, C. M., Su, M. F., Olsson III, R. H., Shaner, E. A., Leseman, Z. C., Serrano, J. R., Phinney, L. M. & El-Kady, I. (2010), 'Reduction in the thermal conductivity of single crystalline silicon by phononic crystal patterning', *Nano Letters* **11**(1), 107–112.

Huberman, S. C. (2013), Phonon Properties in Superlattices, PhD thesis.

Huberman, S. C., Larkin, J. M., McGaughey, A. J. & Amon, C. H. (2013), 'Disruption of superlattice phonons by interfacial mixing', *Physical Review B* **88**(15), 155311.

Kaviany, M. (2014), *Heat transfer physics*, Cambridge University Press.

Kim, W. & Majumdar, A. (2006), 'Phonon scattering cross section of polydispersed spherical nanoparticles', *Journal of Applied Physics* **99**(8), 084306.

Klemens, P. (1955), 'The scattering of low-frequency lattice waves by static imperfections', *Proceedings of the Physical Society. Section A* **68**(12), 1113.

Klemens, P. (1958), 'Thermal conductivity and lattice vibrational modes', *Solid State Physics* **7**, 1–98.

Knight, J. C. (2003), 'Photonic crystal fibres', *Nature* **424**(6950), 847–851.

Koh, Y. K., Cao, Y., Cahill, D. G. & Jena, D. (2009), 'Heat-transport mechanisms in superlattices', *Advanced Functional Materials* **19**(4), 610–615.

Landry, E. S. (2009), Thermal transport by phonons across semiconductor interfaces, thin films, and superlattices, PhD thesis, Ph. D. thesis, Carnegie Mellon University, Pittsburgh, PA.

Larkin, J. M. (2013), Vibrational Mode Properties of Disordered Solids from High-Performance Atomistic Simulations and Calculations, PhD thesis, Carnegie Mellon University.

Larkin, J. M. & McGaughey, A. J. (2013), 'Predicting alloy vibrational mode properties using lattice dynamics calculations, molecular dynamics simulations, and the virtual crystal approximation', *Journal of Applied Physics* **114**(2), 023507.

Lee, S.-M., Cahill, D. G. & Venkatasubramanian, R. (1997), 'Thermal conductivity of si–ge superlattices', *Applied Physics Letters* **70**(22), 2957–2959.

Li, B., Tan, K. & Christensen, J. (2017), 'Tailoring the thermal conductivity in nanophononic metamaterials', *Physical Review B* **95**(14), 144305.

Lv, W. & Henry, A. (2016), 'Direct calculation of modal contributions to thermal conductivity via green–kubo modal analysis', *New Journal of Physics* **18**(1), 013028.

Ma, R. & Lukes, J. R. (2018), 'Validity of the isotropic thermal conductivity assumption in supercell lattice dynamics', *Journal of Applied Physics* **123**(6), 065106.

Maldovan, M. (2013*a*), 'Narrow low-frequency spectrum and heat management by thermocrystals', *Physical Review Letters* **110**(2), 025902.

Maldovan, M. (2013*b*), 'Sound and heat revolutions in phononics', *Nature* **503**(7475), 209–217.

Maldovan, M. (2015), 'Phonon wave interference and thermal bandgap materials', *Nature Materials* **14**(7), 667–674.

Marconnet, A. M., Kodama, T., Asheghi, M. & Goodson, K. E. (2012), 'Phonon conduction in periodically porous silicon nanobridges', *Nanoscale and Microscale Thermophysical Engineering* **16**(4), 199–219.

Martín-González, M., Caballero-Calero, O. & Díaz-Chao, P. (2013), 'Nanoengineering thermoelectrics for 21st century: Energy harvesting and other trends in the field', *Renewable and Sustainable Energy Reviews* **24**, 288–305.

McGaughey, A. J. & Kaviany, M. (2004), 'Quantitative validation of the boltzmann transport equation phonon thermal conductivity model under the single-mode relaxation time approximation', *Physical Review B* **69**(9), 094303.

McGaughey, A. & Kaviany, M. (2005), 'Observation and description of phonon interactions in molecular dynamics simulations', *Physical Review B* **71**(18), 184305.

McGaughey, A. & Larkin, J. M. (2014), 'Predicting phonon properties from equilibrium molecular dynamics simulations', *Ann. Rev. Heat Transfer* **17**, 49–87.

Mingo, N., Yang, L., Li, D. & Majumdar, A. (2003), 'Predicting the thermal conductivity of si and ge nanowires', *Nano Letters* **3**(12), 1713–1716.

Mizuno, H., Mossa, S. & Barrat, J.-L. (2015), 'Beating the amorphous limit in thermal conductivity by superlattices design', *Scientific reports* **5**.

Nikitov, S., Tailhades, P. & Tsai, C. (2001), 'Spin waves in periodic magnetic structuresmagnonic crystals', *Journal of Magnetism and Magnetic Materials* **236**(3), 320–330.

Omini, M. & Sparavigna, A. (1995), 'An iterative approach to the phonon boltzmann equation in the theory of thermal conductivity', *Physica B: Condensed Matter* **212**(2), 101–112.

Omini, M. & Sparavigna, A. (1996), 'Beyond the isotropic-model approximation in the theory of thermal conductivity', *Physical Review B* **53**(14), 9064.

Omini, M. & Sparavigna, A. (1997), 'Heat transport in dielectric solids with diamond structure', *NUOVO CIMENTO-SOCIETA ITALIANA DI FISICA SEZIONE D* **19**, 1537–1564.

Qiu, B., Bao, H., Zhang, G., Wu, Y. & Ruan, X. (2012), 'Molecular dynamics simulations of lattice thermal conductivity and spectral phonon mean free path of pbte: Bulk and nanostructures', *Computational Materials Science* **53**(1), 278–285.

Qiu, B., Chen, G. & Tian, Z. (2015), 'Effects of aperiodicity and roughness on coherent heat conduction in superlattices', *Nanoscale and Microscale Thermophysical Engineering* **19**(4), 272–278.

Ravichandran, J., Yadav, A. K., Cheaito, R., Rossen, P. B., Soukiassian, A., Suresha, S., Duda, J. C., Foley, B. M., Lee, C.-H., Zhu, Y. et al. (2014), 'Crossover from incoherent to coherent phonon scattering in epitaxial oxide superlattices', *Nature Materials* **13**(2), 168.

Reinke, C. M., Su, M. F., Davis, B. L., Kim, B., Hussein, M. I., Leseman, Z. C., Olsson-III, R. H. & El-Kady, I. (2011), 'Thermal conductivity prediction of nanoscale phononic crystal slabs using a hybrid lattice dynamics-continuum mechanics technique', *AIP Advances* **1**(4), 041403.

Rybin, M. V., Filonov, D. S., Samusev, K. B., Belov, P. A., Kivshar, Y. S. & Limonov, M. F. (2015), 'Phase diagram for the transition from photonic crystals to dielectric metamaterials', *Nature communications* **6**, 10102.

Schelling, P., Phillpot, S. & Keblinski, P. (2002), 'Phonon wave-packet dynamics at semiconductor interfaces by molecular-dynamics simulation', *Applied Physics Letters* **80**(14), 2484–2486.

Sellan, D. P., Turney, J., McGaughey, A. J. & Amon, C. H. (2010), 'Cross-plane phonon transport in thin films', *Journal of Applied Physics* **108**(11), 113524.

Seyf, H. R., Yates, L., Bougher, T. L., Graham, S., Cola, B. A., Detchprohm, T., Ji,

M.-H., Kim, J., Dupuis, R., Lv, W. et al. (2017), 'Rethinking phonons: The issue of disorder', *npj Computational Materials* **3**(1), 49.

Singh, D., Murthy, J. Y. & Fisher, T. S. (2011), 'Effect of phonon dispersion on thermal conduction across si/ge interfaces', *Journal of Heat Transfer* **133**(12), 122401.

Slack, G. A. & Glassbrenner, C. (1960), 'Thermal conductivity of germanium from 3 k to 1020 k', *Physical Review* **120**(3), 782.

Soukoulis, C. M. & Wegener, M. (2011), 'Past achievements and future challenges in the development of three-dimensional photonic metamaterials', *Nature Photonics* **5**(9), 523–530.

Sparavigna, A. C. (2016), 'The boltzmann equation of phonon thermal transport solved in the relaxation time approximation–ii–data analysis', *Mechanics, Materials Science & Engineering Journal* **2016**(3), 57–66.

Srivastava, G. P. (1990), *The physics of phonons*, CRC press.

Tamura, S., Tanaka, Y. & Maris, H. J. (1999), 'Phonon group velocity and thermal conduction in superlattices', *Physical Review B* **60**(4), 2627.

Tang, J., Wang, H.-T., Lee, D. H., Fardy, M., Huo, Z., Russell, T. P. & Yang, P. (2010), 'Holey silicon as an efficient thermoelectric material', *Nano Letters* **10**(10), 4279–4283.

Turney, J. E. (2009), Predicting phonon properties and thermal conductivity using anharmonic lattice dynamics calculations, PhD thesis, Carnegie Mellon University.

Wang, H., Zeng, H., Li, Q. & Shen, J. (2016), 'Superlattice supertoughness of tin/mn (m= v, nb, ta, mo, and w): First-principles study', *Thin Solid Films* **607**, 59–66.

Wang, P., Casadei, F., Shan, S., Weaver, J. C. & Bertoldi, K. (2014), 'Harnessing buckling to design tunable locally resonant acoustic metamaterials', *Physical Review Letters* **113**(1), 014301.

Ward, A. & Broido, D. (2010), 'Intrinsic phonon relaxation times from first-principles studies of the thermal conductivities of si and ge', *Physical Review B* **81**(8), 085205.

Yang, B. & Chen, G. (2003), 'Partially coherent phonon heat conduction in superlattices', *Physical Review B* **67**(19), 195311.

Yang, L., Yang, N. & Li, B. (2014), 'Extreme low thermal conductivity in nanoscale 3d si phononic crystal with spherical pores', *Nano letters* **14**(4), 1734–1738.

Yu, J.-K., Mitrovic, S., Tham, D., Varghese, J. & Heath, J. R. (2010), 'Reduction of thermal conductivity in phononic nanomesh structures', *Nature Nanotechnology* **5**(10), 718–721.

Zen, N., Puurtinen, T. A., Isotalo, T. J., Chaudhuri, S. & Maasilta, I. J. (2014), 'Engineering thermal conductance using a two-dimensional phononic crystal', *Nature communications* **5**, 3435.

Zhao, H. & Freund, J. (2005), 'Lattice-dynamical calculation of phonon scattering at ideal si–ge interfaces', *Journal of Applied Physics* **97**(2), 024903.

Zhou, Y., Zhang, X. & Hu, M. (2015), 'Quantitatively analyzing phonon spectral contribution of thermal conductivity based on nonequilibrium molecular dynamics simulations. i. from space fourier transform', *Physical Review B* **92**(19), 195204.

Ziman, J. M. (1960), *Electrons and phonons: the theory of transport phenomena in solids*, Oxford university press.